Macromolecules

pubs.acs.org/Macromolecules

Article

Role of Dynamical Asymmetry on the Orientation of Block Copolymers in Shear Flow: Computer Simulation and Experiment

Niklas Blagojevic, Matthias Heck, Manfred Wilhelm,* and Marcus Müller*

Cite This: *Macromolecules* 2024, 57, 8470−8486

Read Online

ACCESS | Metrics & More | Article Recommendations | Supporting Information

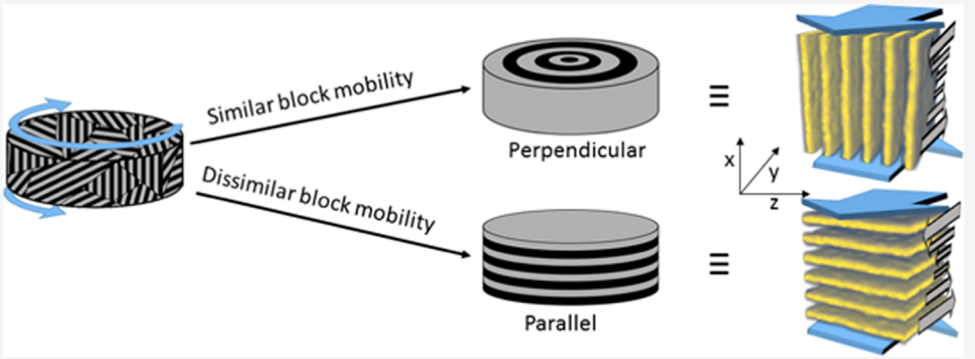

ABSTRACT: The ability of diblock copolymers to self-assemble into periodic microstructures with length scales in the nanometer range offers many opportunities for fundamental research and applications. For practical applications, it is often desirable that the microstructures have a high degree of order on macroscopic length scales and are oriented in a desired direction. This can be achieved in a large volume by shearing the copolymer melt. In experiments, different orientations are observed depending on the copolymer characteristics and the applied shear conditions. However, details of the orientation mechanism under shear are not completely understood. Studying structurally and thermodynamically symmetric, lamellae-forming diblock copolymers by molecular simulation using a highly coarse-grained model, we analyze the effect of dynamical asymmetry on the stable orientation in steady-shear flow. We control the dynamical asymmetry via (i) the segmental friction in our dissipative particle dynamics DPD simulation or via (ii) slip springs, which mimic physical entanglements of the polymers. We study the kinetics of structure formation after a quench from the disordered state in the presence of shear and the ordering of a system, initially comprised of two orthogonally oriented lamellar grains, under shear. In both simulation settings and for both mechanisms of dynamical asymmetry, the perpendicular orientation, where the lamellae normals are perpendicular to the shear gradient, is preferred for approximately equal dynamics of the two blocks, whereas the parallel orientation becomes stable when the ratio of the relaxation times of the blocks exceeds an order of magnitude. We rationalize this finding by the minimum of the Rayleighian, i.e., the energy dissipation rate of the nonequilibrium steady state. We compare these simulation results to experimental diblock copolymer model systems, polystyrene-*b*-poly-2-vinylpyridine, with slightly different glass transition temperatures of the two polymer blocks. Adjustment of the polymer block mobility by different temperatures for alignment experiments confirms the trend toward a parallel orientation with increasing dynamical asymmetry of the polymer blocks, when the rigid lamellae slide past the opposing brushes of the more mobile polymer block.

INTRODUCTION

Diblock copolymers feature multiple interesting, tunable morphologies, which can be designed by simple accessible parameters like the volume fraction and incompatibility of the involved segment types, as well as the molecular topology.[1]

Microphase separation makes these materials ideal candidates for the fabrication of self-assembled nanostructures with repeating patterns in the length scales ranging from a few to 100 nm. For the majority of self-assembly applications, it is of great interest to gain control over the orientation of the spatially modulated morphologies on large length scales.[2,3] Macroscopically, domains may be aligned using external fields such as electrical,[4−21] magnetic,[22,23] or mechanical shear fields[24−33] to form macroscopically anisotropic materials. In this study, lamellae-forming block copolymers (BCPs), that have a similar volume fraction, *f*, of both polymer blocks, are investigated. While the principles that govern the equilibrium

Received: April 25, 2024
Revised: August 13, 2024
Accepted: August 16, 2024
Published: August 28, 2024

https://doi.org/10.1021/acs.macromol.4c00943
Macromolecules 2024, 57, 8470−8486

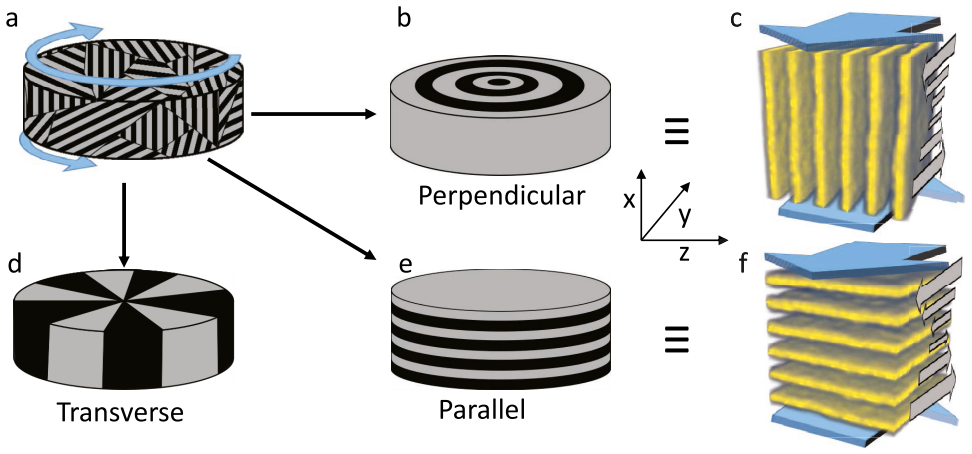

Figure 1. Schematic depiction of the lamellar orientation in our experiments (a, b, d, e) and simulations (c + f). The macroscopically isotropic lamellar morphology of a block copolymer (BCP) (a) can be aligned by shear (indicated by blue arrows) and form a perpendicular (b, c), parallel (e, f) or transverse (d) orientation. For both, the perpendicular and the parallel orientation, the shear flow is parallel to the lamellae. In contrast, for the transverse orientation, the shear flow is orthogonal to the lamellae, making this configuration unstable. In the perpendicular orientation, the shear gradient is within the lamellar planes (i.e., perpendicular to the lamellar normal), whereas in the parallel orientation, it is parallel to the lamellar normal.

phase behavior of BCPs are well established,[1] the effects of processing, such as the application of shear, are only incompletely understood.[34]

A lamellar configuration is characterized by its normal vector but is translationally invariant in the other two dimensions. Steady shear flow, in turn, is described by the shear-flow direction and the gradient direction. As a result there are three distinct orthogonal configurations of lamellae in shear flow: a perpendicular orientation, a parallel orientation, and a transverse orientation, which are depicted in Figure 1.

Several particle-based simulation studies of block copolymers have been performed with different models and techniques.[27−33] In computer simulations, one typically observes the perpendicular orientation of the lamellae to be more stable than the parallel orientation for steady shear.

In experiments, however, until a work by Koppi et al. published in 1992, it was widely accepted that lamellae-forming diblock copolymers only orient in the parallel configuration when sheared.[24] Subsequent research demonstrated that both perpendicular and transverse configurations could also be obtained.[25,35,36] The transverse orientation, see Figure 1d, is only a transient state that eventually transitions to the parallel orientation.[25] The discrepancy between the stability of different orientations in simulation and experiment leads to the question of its fundamental origin.

The above-mentioned computer simulations[27−33,37] studied dynamically symmetric blocks, which exhibit the same segmental dynamics, but this idealization may not be fulfilled in most experiments. Thus, we hypothesize that the observation of the parallel orientation in experiments is an effect of dynamical asymmetry. In the present study we investigate the stability of lamellar orientations under shear flow for diblock copolymers whose blocks exhibit different segmental dynamics.

In the simulations, polymers are modeled within a highly coarse-grained model with soft interactions,[33,37−43] and shear flow in our molecular dynamics (MD) simulations is generated by reverse nonequilibrium molecular dynamics simulation (RNEMDS),[44] which imposes a shear stress. Dynamical asymmetry between the blocks is introduced by two strategies: (i) we control the dynamics by the segmental friction of the dissipative particle dynamics (DPD) thermostat,[40,45] or (ii) we slow down the dynamics of one block by introducing slip springs that mimic entanglements along the corresponding block.[39,41−43,46]

We systematically vary the dynamical asymmetry and employ three different setups to determine the stable lamellar orientation: First, equilibrated lamellae are subjected to a shear flow either parallel or perpendicular to the lamellar normal. In this nonequilibrium steady state, we measure the energy-dissipation rate and predict the stability of the orientations using the Rayleighian.[28,33,47] Second, we study the kinetics of structure formation in an initially disordered BCP melt after a quench across the order−disorder-transition (ODT) in the presence of shear flow, and observe the impact of shear and dynamical asymmetry on the resulting orientation of the lamellae. Third, we examine a metastable system that initially contains two orthogonal grains of equilibrated lamellae−one parallel and the other perpendicular to the shear flow. This system is subjected to shear stress, and we monitor the reorientation kinetics as a function of flow strength and dynamical asymmetry. We will compare our simulation results and predictions with rheological domain-alignment experiments, which are designed to be similar to the simulations. The single-chain dynamics are not directly accessible in our experiments. Instead, we characterize the dynamics of the individual blocks by the temperature difference from their glass transition points.[48−50] A polymer system with similar T_gs of the two polymer blocks−polystyrene-*b*-poly-2-vinylpyridine, PS-*b*-P2VP, where the difference of glass transition temperatures ΔT_g is about 15 °C—is used for the alignment experiments. This slight difference in T_g allows us to control the mobility difference of the polymer blocks in the alignment experiments via the temperature. A quench from the disordered to the lamellar state in the simulation is compared to the cooling from a homogeneous melt to a microphase-separated melt below the order−disorder-transition temperature in experiments. The grain coarsening observed in the simulation with two orthogonally oriented grains is experimentally mimicked

https://doi.org/10.1021/acs.macromol.4c00943
Macromolecules 2024, 57, 8470−8486

by a realignment of the lamellar domains from one orientation to another.

SIMULATION MODEL AND TECHNIQUES

We consider a soft, highly coarse-grained model[33,37,39] of n symmetric AB diblock copolymers in a volume, V. The molecular contour is discretized into $N = 16$ coarse-grained segments or particles. Since each particle represents a large number of monomeric repeating units, the distance distribution between neighboring particles is approximately Gaussian, and we use a harmonic bond potential

$$\frac{V_b(\mathbf{r})}{k_BT} = \frac{1}{2}k_2\mathbf{r}^2 \tag{1}$$

where $\mathbf{r}$ denotes the distance between neighboring particles along the molecular contour. The parameter adopts the value $k_2 = 3/b_0^2 = 5.45/\sigma^2$, where b_0 denotes the root-mean-squared bond length in the absence of nonbonded interactions, in accord with previous studies.[33,37] Further details on the selection of simulation parameters can be found in the Supporting Information. The harmonic bond potential in our highly coarse-grained model is substantially softer as compared to the microscopic, atom−atom bond potential.

A diblock copolymer is comprised of $f_AN = 8$ particles of type A and the same number of B segments. The soft, nonbonded, pairwise interaction between particles represents the effect of excluded-volume interaction between atoms that imparts a finite compressibility onto the dense polymer liquid on the coarse-grained scale, and the repulsion between unlike particle species that gives rise to microphase separation into a lamellar morphology. The nonbonded interactions take the DPD form[38]

$$\frac{V_{nb}(\mathbf{r})}{k_BT} = \begin{cases} \frac{v_{ij}}{2}\left(1 - \frac{|\mathbf{r}|}{\sigma}\right)^2 & \text{for } |\mathbf{r}| < \sigma \\ 0 & \text{for } |\mathbf{r}| \geq \sigma \end{cases} \tag{2}$$

where v_{ij} characterizes the strength of the repulsion between species, i and j, and σ denotes the spatial range of the nonbonded, pairwise interactions. We use the parameter values $v_{AA} = v_{BB} = 1.32k_BT$. In the disordered phase, we set $v_{AB} = v_{AA}$, whereas $v_{AB} = 1.94k_BT > v_{AA}$ for the microphase-separated state. Ignoring liquid-like packing effects of the dense fluid of soft particles and renormalization due to fluctuation effects, we can approximately relate the interaction parameters to a Flory−Huggins interaction and the inverse isothermal compressibility via $v_{AB} \approx \frac{15}{\pi\rho_0}(\kappa + \chi)$, resulting in $\chi N \approx 40$ and $\kappa N \approx 84$, with ρ_0 denoting the particle number density (see Supporting Information for a derivation of the mapping).

The root-mean-squared end-to-end distance of the corresponding homopolymer melt is given by $\sqrt{\langle R_e^2\rangle} = (3.0 \pm 0.1)\sigma$. We employ a rather small invariant degree of polymerization, $\sqrt{\bar{N}} = nR_e^3/V = 32$, corresponding to a particle number density of $\rho_0 = nN/V = 18.96/\sigma^3$ unless otherwise noted. Solely for the study of two differently oriented grains under shear, we employ a smaller value of $\sqrt{\bar{N}} = 19$, in order to lower the free-energy barriers associated with reorientation phenomena.[51]

We use the DPD thermostat[40,45] to perform our simulations in the canonical ensemble with the spatial range σ of the pairwise thermostat. For the evolution of the MD simulation, we use the Velocity-Verlet algorithm[52] with a time step of $\Delta t = 10^{-3}\tau$, where $\tau = \sigma\sqrt{m/k_BT}$, with m being the mass of a particle, denotes the intrinsic time unit of the model. The MD simulations are performed with the simulation program HOOMD-Blue.[53,54] The DPD thermostat accounts for a friction force, $\mathbf{F}_{D,ij}$, due to the relative velocity of a neighboring particle pair as well as for a concomitant pairwise random force. Both forces are related via the fluctuation−dissipation theorem and their strength is controlled by the coefficients γ_{ij}, where $i, j \in [A, B]$ are the different types of the particles. The friction force between two particles i and j reads

$$\mathbf{F}_{D,ij} = -\gamma_{ij}w^2(\mathbf{r}_{ij})(\hat{\mathbf{r}}_{ij}\cdot\mathbf{v}_{ij})\hat{\mathbf{r}}_{ij} \tag{3}$$

with $w(\mathbf{r}) = \max(1 - |\mathbf{r}|/\sigma, 0)$ and velocity difference, $\mathbf{v}_{ij} = \mathbf{v}_i - \mathbf{v}_j$. The distance vector between the particles is $\mathbf{r}_{ij} = \mathbf{r}_i - \mathbf{r}_j$ and $\hat{\mathbf{r}}_{ij} = \mathbf{r}_{ij}/|\mathbf{r}_{ij}|$. The parameter controlling the magnitude of this force, γ_{ij}, depends on the particle types of the pair. The random force between particles of the pair takes the form $\mathbf{F}_{R,ij}(r) = \sqrt{6\gamma_{ij}k_BT/\Delta t}\,w(\mathbf{r}_{ij})\theta_{ij}\hat{\mathbf{r}}_{ij}$, where $-1 \leq \theta_{ij} \leq 1$ is a uniformly distributed random number. We set $\gamma_{AA} = 1\frac{m}{\tau}$, $\gamma_{AB} = (\gamma_{AA} + \gamma_{BB})/2$ and control γ_{BB} to introduce a dynamical asymmetry via the segment-friction difference.

Alternatively, we use slip springs[39,41−43,46] that mimic the effect of entanglements. These slip springs can only form between particles of the dynamically slow block, B, i.e., the B block follows tube-model dynamics, whereas the A block obeys Rouse-like dynamics. For the simulations with slip springs we set $\gamma_{BB} = \gamma_{AA}$. To control the degree of dynamical asymmetry, we vary the slip-spring activity, z_{ss}, which is linearly related to the number of slip springs in the system. As a maximum for the employed z_{ss} we use $z_{ss} = 1$, corresponding to approximately 1.6 slip-spring bonds per total number of particles—i.e., counting A and B segments—in an equilibrated, disordered BCP system with $\rho_0 = 18.96/\sigma^3$. This corresponds to the bosonic slip-spring model, in which multiple slip-spring bonds can attach to a particle, unlike fermionic models that restrict attachment to a maximum of one slip-spring bond per particle.[55,56] Particles connected by a transient slip-spring bond interact via a finite extensible nonlinear elastic (FENE) potential

$$V_{ss}(\mathbf{r}) = -\frac{k_{ss}r_{ss}^2}{2}\ln\left[1 - \left(\frac{|\mathbf{r}|}{r_{ss}}\right)^2\right] \tag{4}$$

for $|\mathbf{r}| < r_{ss}$ and 0 otherwise. We set $k_{ss} = k_2$ to the same value used for the harmonic bonds along the polymer chain and $r_{ss} = \sigma$. To prepare systems with slip springs, we initially equilibrate the systems without slip springs in the desired state without shear, e.g., in a disordered or lamellar state. Then, slip springs are added to the system via a grand-canonical MC scheme, sampling the partition function

$$Z \propto \int \mathcal{D}(\{\mathbf{r}_i\})\exp\left(-\frac{V_0 + \sum_{i_B<j_B} V_{comp}}{k_BT}\right) \prod_{i_B<j_B}\sum_{n_{ij}=0}^{\infty}\frac{z^{n_{ij}}}{n_{ij}!}\exp\left(-n_{ij}\frac{V_{ss}(\mathbf{r}_{ij})}{k_BT}\right) \tag{5}$$

https://doi.org/10.1021/acs.macromol.4c00943
Macromolecules 2024, 57, 8470−8486

Table 1. Measured Rouse Times of Copolymers, τ_R, Rouse Times of the Slow Blocks in a Disordered Blend Containing *A*-Type and *B*-Type Homopolymers, $\tau_{R,B}^{\text{block}}$, and Rouse Times of the Slow Blocks in Pure Systems Containing Solely Homopolymers of the Slow *B*-Type, $\tau_{R,B}^{\text{h-poly}}$[a]

system	τ_R [τ]	$\tau_{R,B}^{\text{block}}$ [τ]	$\tau_{R,B}^{\text{h-poly}}$ [τ]	$\eta_0 \left[\frac{k_B T \tau}{\sigma^3}\right]$	$\eta_{0,B}^{\text{h-poly}} \left[\frac{k_B T \tau}{\sigma^3}\right]$
$\gamma_{AA} = \gamma_{BB} = 1$, $z_{ss} = 0$	13	3	3	28 ± 1	18 ± 1
$\gamma_{AA} = \gamma_{BB} = 1$, $z_{ss} = 0.1$	60	12	33	122 ± 4	210 ± 8
$\gamma_{AA} = \gamma_{BB} = 1$, $z_{ss} = 0.2$	260	31	105	411 ± 14	670 ± 64
$\gamma_{AA} = \gamma_{BB} = 1$, $z_{ss} = 0.4$	990	100	343	1602 ± 55	2527 ± 95
$\gamma_{AA} = \gamma_{BB} = 1$, $z_{ss} = 1.0$	10 500	442	1334	11 152 ± 384	10 410 ± 390
$\gamma_{AA} = 1$, $\gamma_{BB} = 100$, $z_{ss} = 0$	460	76	243	966 ± 33	1380 ± 52

[a]For the measurement of the Rouse times of the slow blocks, we performed measurements of the block self-diffusion coefficient. For the measurement of $\tau_{R,B}^{\text{h-poly}}$, we consider a system where all homopolymers are of the slow type, *B*, and for the measurement of $\tau_{R,B}^{\text{block}}$, one half of all polymers are of the slow type, *B*, and the remaining half of type *A*. Additionally, we compile the zero-shear viscosity, $\eta_0 = \lim_{j_p \to 0} j_p/\dot{\gamma}$ for different systems in a disordered state containing copolymers for varying degrees of asymmetry, as well as for a system containing solely homopolymers of the slow type, $\eta_{0,B}^{\text{h-poly}}$.

where $\mathcal{D}(\{\mathbf{r}_i\})$ runs over all molecular configurations, V_0, represents the potential energy due to bonded and nonbonded interactions. The product $i_B < j_B$ runs over all pairs that can be connected by slip springs, which corresponds to pairs of different *B* particles that are not direct neighbors along the polymer backbone, and n_{ij} denotes the number of slip springs connecting the pair *ij*. To leave the equilibrium properties of systems with slip springs unaltered, a compensating pair-repulsion is introduced that acts between all particles that can be connected by slip springs:[46]

$$V_{\text{comp}}(\mathbf{r}_{ij}) = k_B T z \exp\left(-\frac{V_{\text{ss}}(\mathbf{r}_{ij})}{k_B T}\right) \tag{6}$$

After the slip springs have been added to an initially equilibrated configuration according to eq 5, we perform DPD simulations as described before using the Velocity-Verlet algorithm[52] and additionally update the slip-spring configurations using MC moves in a regular interval every $1000\Delta t = 1\tau$ integration steps to simulate the dynamics of the slip springs. This interval was chosen so that the slip-spring displacement by hopping is comparable to the average segment displacement in this period, with the root-mean-squared segment displacement during this interval being $\sqrt{g_1(\tau)} \approx 0.9\sigma$. We apply two different MC moves: (i) The slide-MC move allows slip-spring anchors to slide along the molecular backbone, i.e., the attachment of a slip spring moves to a neighboring segment along the polymer backbone. This mimics the slithering-snake-like motion of the entangled block. (ii) Slip springs can be created or destroyed if one attachment point is at a chain end. This is implemented as a grandcanonical MC move that mimics constraint renewal (at the chain end) and constraint release (at the other attachment point of the slip spring). Both MC moves sample the partition function eq 5.

In our simulations, the shear flow is directed along the *y*-axis, and the shear gradient along the *x*-axis. To generate shear flow, we use the RNEMDS scheme,[44] where a shear stress is imposed by a local momentum flux and the resulting shear flow is observed. To this end, the simulation box is divided into slabs along the direction of the shear gradient, *x*-direction, with a slab thickness of 1σ. This size was chosen to minimize local perturbation caused by momentum exchanges while ensuring there are sufficiently many particles in each slab for effective momentum transfer. Momentum transfer occurs between two predetermined slabs that are spaced half the box length, $L_x/2$, apart. The momentum transfer involves swapping the momentum of the particle with the highest velocity in shear-flow direction, $\max(mv_y)$, in one slab with that of the particle with the lowest, $\min(mv_y)$, in the other slab. The exchanged momentum, Δp, generates a momentum flux that defines the shear stress, $j_p = \frac{\Delta p}{2\Delta t L_y L_z}$, which is monitored. This swapping-procedure is repeated in each simulation time step until the total momentum flux corresponds to the desired strength of the shear stress given as input parameter.

A characteristic relaxation time scale is the Rouse time $\tau_R = R_e^2/(3\pi^2 D)$, where D denotes the measured self-diffusion coefficient in the disordered melt, $\chi N = 0$. We present the measured Rouse times in Table 1. In this table we additionally compile the measured Rouse times for the dynamically slow blocks, as well as the measured zero-shear viscosities for the different systems, which we calculate as ratio of the applied shear stress to the resulting shear rate, $\eta_0 = \lim_{j_p \to 0} j_p/\dot{\gamma}$.

For the calculations of the shear rates, we monitor a grid-based, one-dimensional, averaged velocity profile, $v_y(x)$, in the direction of the shear gradient with a grid spacing of σ. We estimate the shear rate from the average gradient of the velocity profile, i.e., $\dot{\gamma} = \left\langle \frac{\partial v_y(x)}{\partial x} \right\rangle$, omitting regions of width $3\sigma \approx R_e$ around the momentum-exchange zones.

For generating initial configurations with the desired morphologies, e.g., an equilibrated lamellar configuration, we initially use a short DPD simulation with external fields that restrain the densities to the desired morphology.[51] After the particles have adapted to the respective morphology, we equilibrate the system using a DPD simulation without the external fields. We also use this procedure to determine the equilibrium lamellar spacing by initializing different simulations with a fixed number of lamellar domains but varying system geometry. We then measure the pressure, which is isotropic at the equilibrium spacing.

EXPERIMENTAL SYSTEMS AND TECHNIQUES

For experimental systems, the monomer friction parameter γ as well as the number of entanglements cannot be chosen freely. The type of polymer dictates γ, and the number of entanglements is set by the polymer's entanglement molecular weight M_e and its specific molecular weight. The mobility of a homopolymer chain increases nonlinearly with increasing temperature above its glass transition

https://doi.org/10.1021/acs.macromol.4c00943
Macromolecules 2024, 57, 8470−8486

temperature, T_g, and can be described, for example, by the Williams−Landell−Ferry equation.[48,49] Thus, the mobility difference between the polymer blocks of a block copolymer may be tuned by exploiting different T_g values and the resulting distances between T_g and the temperature of domain-alignment experiments. The polymer blocks in polystyrene-*b*-poly-2-vinylpyridine (PS-*b*-P2VP) have rather similar T_gs, and thus the mobility difference can be adjusted from a high dynamical asymmetry close to the higher T_g of the two polymer blocks toward a dynamically symmetric system at higher temperatures. Polymer samples with polymer blocks below their entanglement molecular weight were chosen so that entanglements do not act as an additional topological constraint for the movement of polymer chains. This eliminates an additional influence parameter on the realized orientation of the lamellae in the experimental systems.[36] The absence of entanglements results in viscoelastic behavior dominated by viscous rather than elastic response, as observed in the master curves for the samples of this study in the Supporting Information. The samples in this study are denoted by the abbreviated polymer name and the number-average molecular weight, M_n, in kg/mol of the individual polymer blocks. For example, a polystyrene-*b*-poly-2-vinylpyridine with M_n = 10 kg/mol in each block is named PS(10.0)P2VP(10.0).

Synthesis. All samples were synthesized using anionic polymerization techniques, which are described in detail in literature.[57,58] Detailed information on the used reagents and their purification can be found in the Supporting Information. Two slightly different synthetic routes were used for the synthesis of the PS-*b*-P2VP samples used in this study, which are displayed in Figure 2.

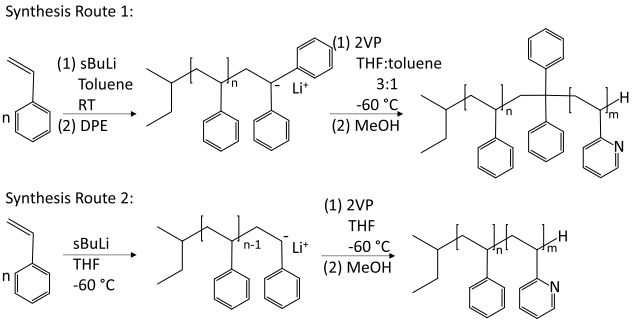

Figure 2. Two synthetic routes were used for the BCP samples of this study. Route 1: The PS block was synthesized in a non polar solvent for a slow polymerization and low Đ of the PS block. The addition of 1,1-diphenylethylene (DPE) is supposed to suppress side reactions when adding 2VP. For solubility reasons tetrahydrofuran (THF) has to be added for the synthesis of the P2VP block. Route 2: The PS block and the P2VP block were both synthesized in the same solvent and no DPE was added in order to conduct the reaction with as little steps as possible, to minimize possible sources of contamination by opening the reaction flask and introducing additional solvents or reactants.

Route 1: The PS block was synthesized in toluene at ambient temperatures inside an ampule. This was done to keep the dispersity, Đ, of the polystyrene block as low as possible. In order to reduce the reactivity of the macroanion, 1,1-diphenylethylene (DPE) was added and the reaction mixture was stirred for 2 h. Please be aware that this addition of DPE might change local mobility and consequently T_{ODT}, see also Table 2. Prior to the synthesis of the P2VP block, THF was distilled into a reaction flask or added from an ampule (9:1 THF/Toluene, e.g., 100 mL for 7 g PS-*b*-P2VP). The comparable polar THF was added for solubility reasons. The polystyrene solution was added to the THF and cooled to −50 °C to prevent side reactions of the reactive macroanion and the THF. Subsequently, the 2VP was added under argon counter flow. The reaction mixture was stirred for 1 h at −50 °C and then stirred for 24 h at room temperature. The reaction was terminated by the addition of degassed methanol.

Route 2: The PS- and P2VP blocks were both synthesized in THF at −60 °C and no DPE was added after the synthesis of the PS block in order to minimize the possibility of contaminations by opening the reaction flask and introducing additional solvents and reagents. The synthesis of the PS-block was conducted under vigorous stirring for approximately 10 min and after an aliquot was drawn for characterization, the 2VP monomer was added to the solution of PS-macroanions directly. The reaction was conducted for 10 additional minutes and then terminated by degassed methanol.

The product of both synthetic routes was precipitated in cold low boiling petroleum ether and dried at ca. 70 °C under reduced pressure.

Sample Characterization. *Molecular Characterization.* The molecular weight of the polymer samples was determined via size exclusion chromatography (SEC). The SEC equipment was from Polymer Standard Service, (Mainz, Germany) specifically the Agilent 1200 series. Two PSS SDV Lux 300 × 8 mm i. d. columns with pore sizes of 10^3 and 10^5 Å were used. The solvent/mobile phase was THF stabilized with 250 ppm BHT at 25 °C with a flow rate of 1 mL min^{-1}. A Bruker Avance lll Microbay 400 MHz spectrometer was used to determine the molecular composition of the block copolymer samples in addition to the SEC-NMR measurements. The samples were dissolved in deuterated chloroform ($CDCl_3$, 99.8%, Sigma-Aldrich) for the NMR experiments and signals were referenced to the solvent peak at δ = 7.26 ppm. Characteristic peaks at δ = 6.2 to 7.3 ppm (aromatic; 5H for PS; 3H for P2VP) in relation to a peak at δ = 8.3 ppm (aromatic; 1H for P2VP) were used to calculate the molecular composition of the PS-*b*-P2VP BCP samples.

Polymer Samples. The PS-*b*-P2VP samples are chosen to be phase separated and to be in a molecular weight range, in which a T_{ODT} is experimentally accessible. The sample PS(8.4)P2VP(8.6) exhibits an unusually high T_{ODT} compared to the other PS-*b*-P2VP samples used in this study. This may be explained by the different synthetic procedure of this sample, in which the bulky monomer DPE was used to reduce the reactivity of the PS macroanion and to prevent side reactions at the pyridine ring.[60−62] Minor differences in Đ or difference in molecular weight, cannot explain the observed deviations from the expected T_{ODT}. The bulky DPE, being covalently bound directly between PS and P2VP, can explain the higher T_{ODT} for this

Table 2. Number Average M_n, Weight Average Molecular Weight M_w, Dispersity Đ, Volume Fraction of the PS-Block f_{PS}, Glass Transition Temperature T_g of the Individual Polymer Blocks and Order Disorder Transition Temperature T_{ODT}[a]

sample code	$M_{n,PS}$ [g mol^{-1}]	$M_{n,P2VP}$ [g mol^{-1}]	Đ	f_{PS}	$T_{g,PS}$ [°C]	$T_{g,P2VP}$ [°C]	T_{ODT} [°C]
PS(7.2)P2VP(7.9)[2]	7200	7900	1.07	0.50	96.2	82.8	162
PS(8.4)P2VP(8.6)[1]	8400	8600	1.08	0.51	94.8	79.2	226
PS(8.9)P2VP(9.4)[2]	8900	9400	1.14	0.51	97.9	89.9	168
PS(13.1)P2VP(13.2)[2]	13 100	13 200	1.12	0.52	99.1	79.4	

[a]The samples are labeled by the abbreviation of the polymer of the respective polymer block and its molecular weight in kg mol^{-1} in parentheses. The PS block and Đ of the BCP were obtained by SEC and $M_{n,P2VP}$ of the P2VP block was calculated from characteristic peaks in NMR spectra. For the calculation of f_{PS}, a density ρ of 1.03 g/cm^3 and 1.13 g/cm^3 was used for PS and P2VP respectively.[59] Different synthetic routes, see Figure 2, were used and are listed at the sample code. The high T_{ODT} of PS(8.4)P2VP(8.6) is explained by an additional reagent, which is incorporated into the polymer chain as a monomer unit at the interface of the two polymer blocks.

https://doi.org/10.1021/acs.macromol.4c00943
Macromolecules 2024, 57, 8470−8486

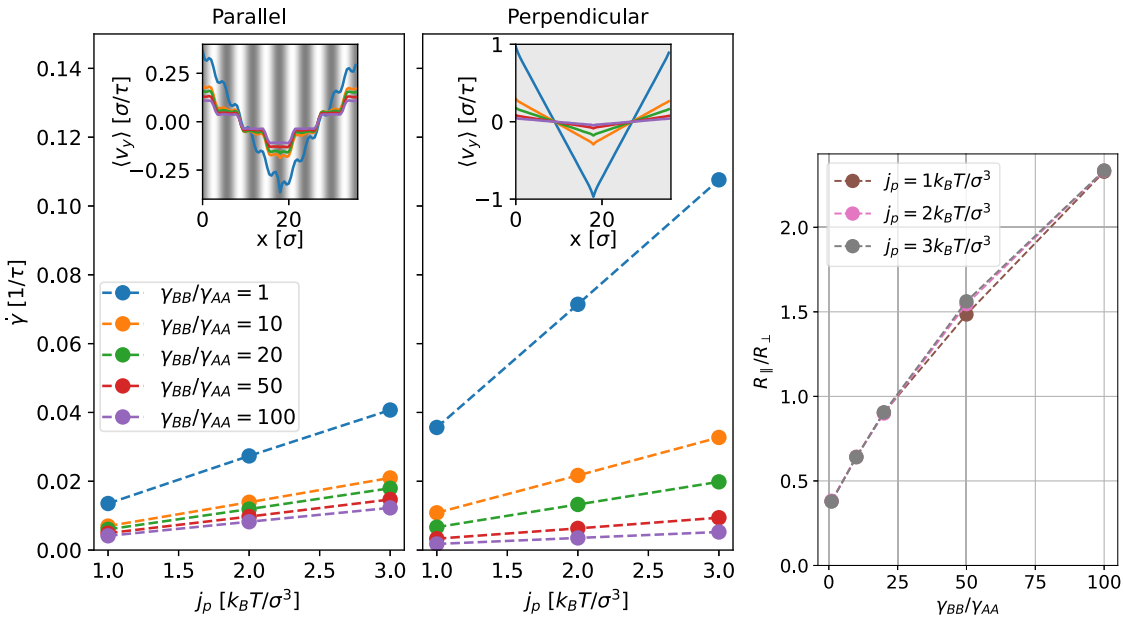

Figure 3. Left: Measured shear rate, $\dot{\gamma}$, as a function of the shear stress, j_p in both lamellar orientations for asymmetric dynamics introduced via segmental friction, γ_{BB}/γ_{AA}. The insets show the average particle velocity $\langle v_y \rangle$ as a function of the position along the shear-gradient axis, x, for $j_p = 3k_BT/\sigma^3$ and varying dynamical asymmetry, while the shading of the background indicates the position of the lamellae. The darker regions correspond to domains of the dynamically slow block. Right: Ratio of the Rayleighians in the two orientations as a function of frictional asymmetry for different shear stresses, j_p.

specific synthetic route. DPE is known to be able to stiffen a polymer chain by the two bulky aromatic rings.[63] The stiffening of the polymer chain directly at the connection of the PS and P2VP, separates the polymer blocks directly at their junction, which may shift the ODT toward higher temperature, as the DPE prefers being at the interface.

Morphological Characterization. To prove phase separation in the block copolymer, differential scanning calorimetry (DSC) measurements were conducted on a TA Q200 differential scanning calorimeter. The temperature ramp rate was 10 K min^{-1}. Thermal history was erased by heating and annealing the sample and data of the second heating run was used. Small angle X-ray (SAXS) measurements were conducted on a Hecus S3-Micro X-ray system with a point microfocus source, 2D-X-ray mirrors, and a two-dimensional CCD-detector from Photonic Science. A PW-H HKP300 press from P/O/Weber (Remshalden, Germany) was used for the sample preparation, while vacuum was applied during preparation to avoid thermal degradation.

Depth-Dependent SAXS Measurements. The orientation in dependence on the distance to the surface (= depth) was determined by placing a piece of the aligned sample in the tangential direction on one of the surfaces, which touched the rheometer tool's metal surface in the sample mount, see Figure SI12. While the normal direction is blind toward parallel oriented lamellae (only scattering signals of the perpendicular and the transverse orientation can be detected) and the radial direction toward perpendicular oriented lamellae (only scattering signals of the parallel and transverse orientation can be detected), scattering signals of both orientations can be detected in the tangential direction in the same scattering experiment. The scattering signals of the sample in the tangential direction at 90 and 270° are cut by the beam stopper in the used setup. The sample was moved with the mount toward the X-ray beam until a scattering pattern appeared, which was considered to be the surface of the sample. The mount was moved step by step through the beam and diffractograms were taken at equidistant depths. The number of scattering experiments varied from 14 to 20 depending on the sample thickness and thus the depth between one experiment to the next was increased about 65 μm.

Domain Alignment Experiments. Oscillatory shear measurements and domain alignment experiments were performed on a strain controlled ARES G2 rheometer (TA Instruments) equipped with a force rebalance transducer (FRT), capable of measuring a torque of 50 nNm to 200 mNm. Orientation experiments were conducted with parallel plate tools with 13 or 25 mm in diameter to have well-defined directions for SAXS analysis, for in situ dielectric measurements, or for a combination of both. Broadband dielectric spectroscopy (BDS) measurements were carried out using a Novocontrol high-resolution α dielectric analyzer Concept 40 allowing a frequency range of 10^{-3} to 10^7 Hz. The dielectric measurement cell rheo-dielectric combination enables the in situ monitoring of orientation processes in block copolymers. A detailed description of this technique applied to block copolymers can be found in the literature.[64,65] The dielectric spectrometer is coupled to the ARES G2 rheometer, as described in detail elsewhere, in order to be able to measure the impact of shear on polymer melts in situ.[64,66]

RESULTS

First we present the results of the molecular simulations and subsequently discuss the experimental findings.

Shear Flow in Lamellar Configurations. We determine the equilibrium lamellar spacing, L_0, in the absence of shear by the requirement that the pressure is isotropic. This yields $L_0 = (6 \pm 0.2)\ \sigma \approx (2 \pm 0.1)\ R_e$ (with R_e denoting the end-to-end distance in a disordered melt), in agreement with the prediction, $L_0 = 1.94R_e$ of self-consistent field theory for Gaussian chains at $\chi N = 40$.

In the following, we consider a cubic box of size $(36\ \sigma)^3$ with 6 lamellae. The shear flow is oriented in y-direction, the shear gradient in x-direction, and we investigate two lamellar orientations: (i) The parallel orientation with the lamellar normal vector parallel to the shear gradient direction, x, and (ii) the perpendicular orientation where the normal vector is parallel to the z-direction (see Figure 1).

In order to determine the stable orientation, we consider the Rayleighian, R, which adopts a minimum in the non-equilibrium steady state. R is comprised of the temporal change of the free energy, F, which is negligible in a nonequilibrium steady state, and the rate of energy dissipation,

https://doi.org/10.1021/acs.macromol.4c00943
Macromolecules 2024, 57, 8470−8486

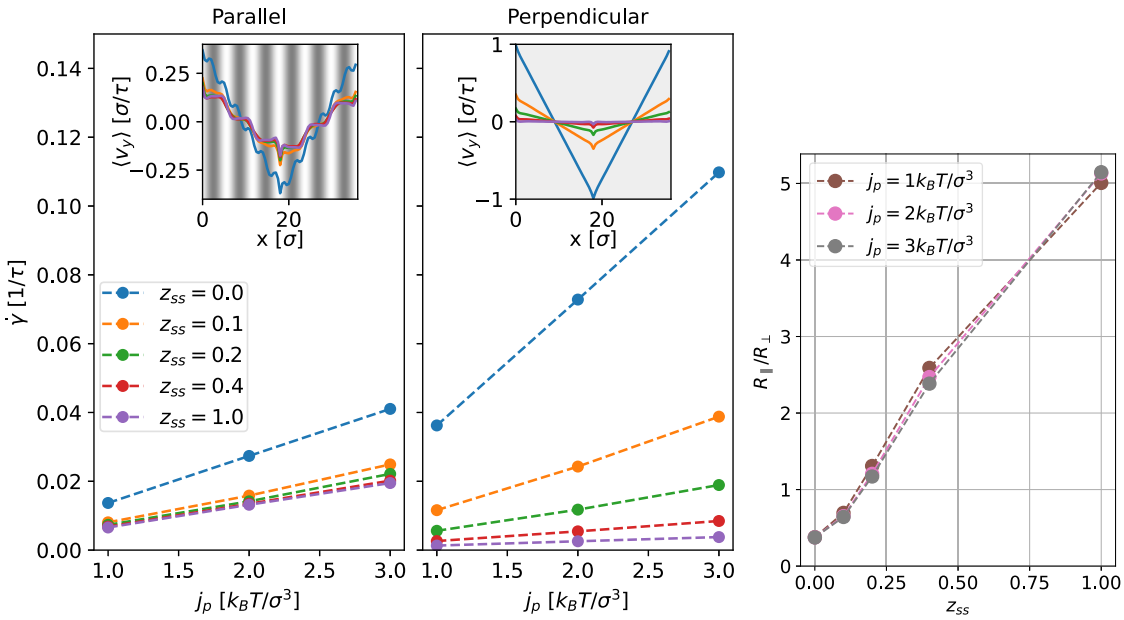

Figure 4. Left: Measured shear rate, $\dot{\gamma}$, as a function of the shear stress, j_p in both lamellar orientations for asymmetric dynamics introduced via slip-spring fugacity, z_{ss}. The insets show the average particle velocity $\langle v_y \rangle$ as a function of the position along the shear-gradient axis, x, for $j_p = 3k_BT/\sigma^3$ and varying dynamical asymmetry. The shading of the background indicates the position of the lamellae, with darker regions corresponding to domains of the dynamically slow block. Right: Ratio of the Rayleighians in the two orientations as a function of the slip-spring activity in the B-block for different shear stresses, j_p.

ΣT, by hydrodynamic flow. For a system with controlled stress,[33] the Rayleighian takes the form

$$R(j_p) = \dot{F} - \frac{1}{2}\Sigma T(j_p) = -\frac{1}{2}\int \mathrm{d}\mathbf{r}\, j_p \dot{\gamma}(j_p) \tag{7}$$

For a given imposed shear stress, j_p, we measure the shear rate, $\dot{\gamma}(j_p)$, after the shear-start-up phase has ended and a steady shear state has been established. This nonequilibrium steady state is achieved once the shear rate and the chain extension have reached time-independent averages. The duration of the shear-start-up phase increases with the characteristic time scale of the system (cf. Table 1) but takes at most 100τ for the studied systems.

For $0 < j_p\sigma^3/k_BT \leq 3.0$ both lamellar orientations are (meta)stable when we introduce the asymmetric dynamics via the B-segment friction, i.e., no reorientation is observed within simulation of duration $50\,000\tau$. Only minor topological changes are detectable in the slip-spring simulations for large values of z_{ss} and $j_p\sigma^3/k_BT \geq 2$, including buckling of lamellae in the parallel configuration and a V-shaped wrinkling of lamellae in the perpendicular configuration.

The shear rates for both orientations and the estimated values for the ratio, $R_\parallel/R_\perp$, of the Rayleighians measured for parallel and perpendicular orientations are presented in Figure 3 for varying segmental frictions, γ_{BB}, and in Figure 4 for varying values of slip-spring activity, z_{ss}, in the B-block.

In all cases, we observe (i) a linear relation between measured shear rate, $\dot{\gamma}$, and imposed shear stress, j_p, indicating that the simulation data correspond to the linear-response regime and (ii) a decrease of $\dot{\gamma}$ as the B-block becomes slower at fixed shear stress. Independent of how the dynamical asymmetric is brought about, this decrease of shear rate is much more pronounced in the perpendicular orientation than in the parallel orientation. In fact, in the parallel orientation, $\dot{\gamma}$, appears to approach a finite value at fixed shear stress as the dynamics of the B-block arrests. In this limit, there is no velocity gradient in the B-lamellae, i.e., the B-lamellae move as integrated plates,[35] and the A-lamellae resemble two opposing brushes, sliding past each other. In the perpendicular orientation, however, the shear gradient is oriented along the lamellar planes, i.e., there must (also) be a velocity gradient in the B lamellae, which becomes the smaller the slower the B-block is.

Since the Rayleighian of the stress-controlled simulation is negative, the system that maximizes the absolute value of the Rayleighian is stable. The threshold value, $R_\parallel/R_\perp = 1$, that marks the transition from the perpendicular orientation—stable for small dynamical asymmetry—to the parallel orientation—stable for high asymmetry—is achieved at $\gamma_{BB}/\gamma_{AA} \approx 25$ or $z_{ss} \approx 0.15$, respectively.

For dynamically symmetric copolymers, $\gamma_{BB}/\gamma_{AA} = 1$ with $z_{ss} = 0$, the ratio between the Rayleighians is $R_\parallel/R_\perp \approx 0.4$. The inverse value of this, $R_\parallel/R_\perp \approx 2.5$, is approximately attained for $\gamma_{BB}/\gamma_{AA} = 100$ or $z_{ss} = 0.4$, where the parallel orientation should become significantly more stable than the perpendicular one. Additionally, we present the data for the ratio of the Rayleighians as a function of the ratio of relaxation times of the blocks, $\tau^P_{R,B}/\tau^P_{R,A}$, in Figure 5. Notably, the data of $R_\parallel/R_\perp$ for the two qualitatively different mechanisms, by which the asymmetry in the dynamics is implemented, approximately overlap. Here, a small deviation is to be expected as the dynamic interaction between A- and B-particles is directly affected when dynamical asymmetry is introduced by variation of γ_{BB} (because $\gamma_{AB} = (\gamma_{BB} + \gamma_{AA})/2$), whereas there is no comparable effect when we introduce the dynamical asymmetry by variation of z_{ss}. Thus, the block relaxation time appears to be a rather robust measure of dynamical asymmetry.

Quench from the Disordered State in the Presence of Shear Flow. While the simulations of lamellae in shear flow provided an estimate of the stable orientation via the Rayleighian, we did not observe a reorientation of the

https://doi.org/10.1021/acs.macromol.4c00943
Macromolecules 2024, 57, 8470−8486

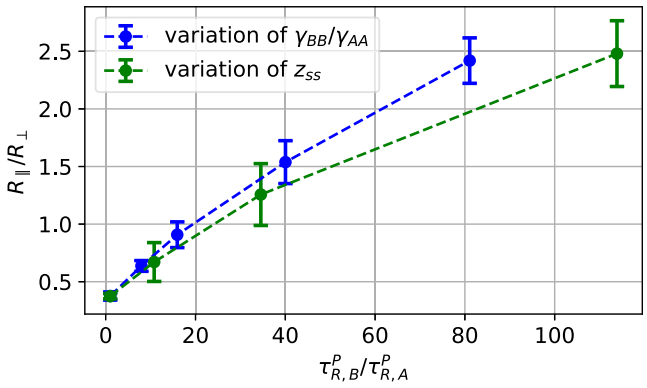

Figure 5. Comparison of the ratio of the Rayleighians in the two orientations for the two different methods of dynamical asymmetry: variation of γ_{BB}/γ_{AA} or variation of z_{ss}. We set $\gamma_{AA} = 1$ for both methods. The data is shown as a function of the ratio of the relaxation times of the slow *B*-block and the fast *A*-block, $\tau^P_{R,B}/\tau^P_{R,A}$, measured in pure *A*- or *B*-homopolymer melts, respectively (cf. Table 1). The latter corresponds to the *A*- and *B*-domains in the strongly segregated, lamellar system.

metastable orientation in the course of our simulations. In order to obtain direct evidence for the stable orientation, we consider a quench from the disordered state across the ODT in the presence of shear.

Shear Flow in a Disordered State. To this end, we first equilibrate a disordered system at vanishing incompatibility, $\chi N = 0$, between the blocks. Then, we subject it to shear stress, $0 < j_p\sigma^3/k_BT \leq 3.0$, which deforms the chain configurations. We study various values of slip-spring activities, z_{ss}, and additionally consider the highest friction contrast, $\gamma_{BB}/\gamma_{AA} = 100$. After the disordered system has attained its non-equilibrium steady state, we investigate the chain deformation.

The stretching of homopolymers in a steady shear flow has been analytically studied within the Rouse model.[67] For weak flow, the chains stretch in the velocity direction, *y*, and the mean-squared chain extension scales as $R^2_e(\dot\gamma)/R^2_e(0) - 1 \sim \mathrm{Wi}^2$, where the Weissenberg number $\mathrm{Wi} = \dot\gamma\tau_R$ measures the shear rate in units of Rouse relaxation time.

In Figure 6 we present $R^2_e(\dot\gamma)/R^2_e(0) - 1$ as a function of the squared Weissenberg number. Although we consider the total relaxation time, τ_R, obtained from the center-of-mass self-diffusion coefficient of the dynamically asymmetric diblock copolymer and consider the total end-to-end distance, the data are approximately compatible with the linear-response behavior.

As one would expect, the shear flow stretches the dynamically slow *B*-block more than the fast block because, at the same shear rate $\dot\gamma$, the Weissenberg number of the *B*-block is larger than that of the *A*-block. This behavior is illustrated in the inset of Figure 6. When plotting the data against the squared Weissenberg number of the slow block, $\mathrm{Wi}^2_B = (\dot\gamma\tau^B_{R,B})^2$, the normalized stretching of the *B*-block in the regime of intermediate dynamical asymmetry, $0.1 \leq z \leq 0.4$ and $\gamma_{BB}/\gamma_{AA} = 100$, primarily depends on its Weissenberg number and is rather independent from its dynamics, Rouse-like for $z_{ss} = 0$ or topologically constraint for $z_{ss} > 0$, respectively. A small deviation between the different curves is expected, however, because the simulations are performed for diblock copolymers, where the *A*-block, bound to the *B*-block, may directly affect the stretching of the *B*-block, depending on the dynamical asymmetry. Taken together with Figure 5, these findings indicate that the studied properties of dynamically asymmetric BCP systems are rather universal.

Structure Formation after a Quench. After a steady flow has been established in the disordered state, we perform a quench to the microphase-separated state, $\chi N \approx 40$. To this end, we linearly increase the incompatibility parameter, $\nu_{AB} - \nu_{AA}$, over a period of 500τ, starting from zero to its final value that corresponds to $\chi N \approx 40$. The applied shear stress, j_p, is kept constant.

In Figure 7 we present snapshots of the morphologies after selected times. Again, we systematically vary the slip-spring activity in the *B*-block and, additionally, consider one large segmental friction contrast, $\gamma_{BB}/\gamma_{AA} = 100$. The panels show the density of one block averaged over the box dimension along the shear-flow direction, *y*. For small dynamical asymmetries, $z_{ss} \leq 0.05$, a strong prevalence of perpendicularly oriented lamellae is observed, whereas for large dynamical asymmetries, $z_{ss} \geq 0.2$ or $\gamma_{BB}/\gamma_{AA} = 100$, the parallel orientation is preferred. This direct observation corroborates the prediction of the Rayleighian (see Figures 3 and 4). The

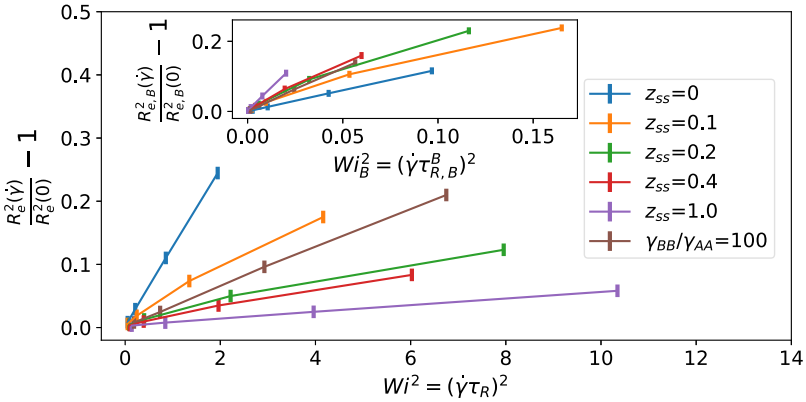

Figure 6. Normalized chain extension, $R^2_e(\dot\gamma)/R^2_e(0) - 1$, in a disordered but dynamically asymmetric diblock copolymer melt for various slip-spring activities z_{ss} at $\gamma_{BB} = \gamma_{AA}$ or $\gamma_{BB}/\gamma_{AA} = 100$ and $z_{ss} = 0$, as a function of the squared Weissenberg number, $\mathrm{Wi}^2 = (\dot\gamma\tau_R)^2$. The steady-state shear flow was generated by imposing shear stresses in the range $0.5 \leq j_p\,\sigma^3/k_BT \leq 3.0$. Inset: Normalized chain extension, $R^2_{e,B}(\dot\gamma)/R^2_{e,B}(0) - 1$, of the slow *B*-block in the diblock copolymer melt as a function of its squared Weissenberg number, $\mathrm{Wi}^2_B = (\dot\gamma\,\tau^B_{R,B})^2$, where the relaxation time of the slow block was calculated in a disordered blend containing *A*- and *B*-homopolymers (cf. Table 1).

https://doi.org/10.1021/acs.macromol.4c00943
Macromolecules 2024, 57, 8470−8486

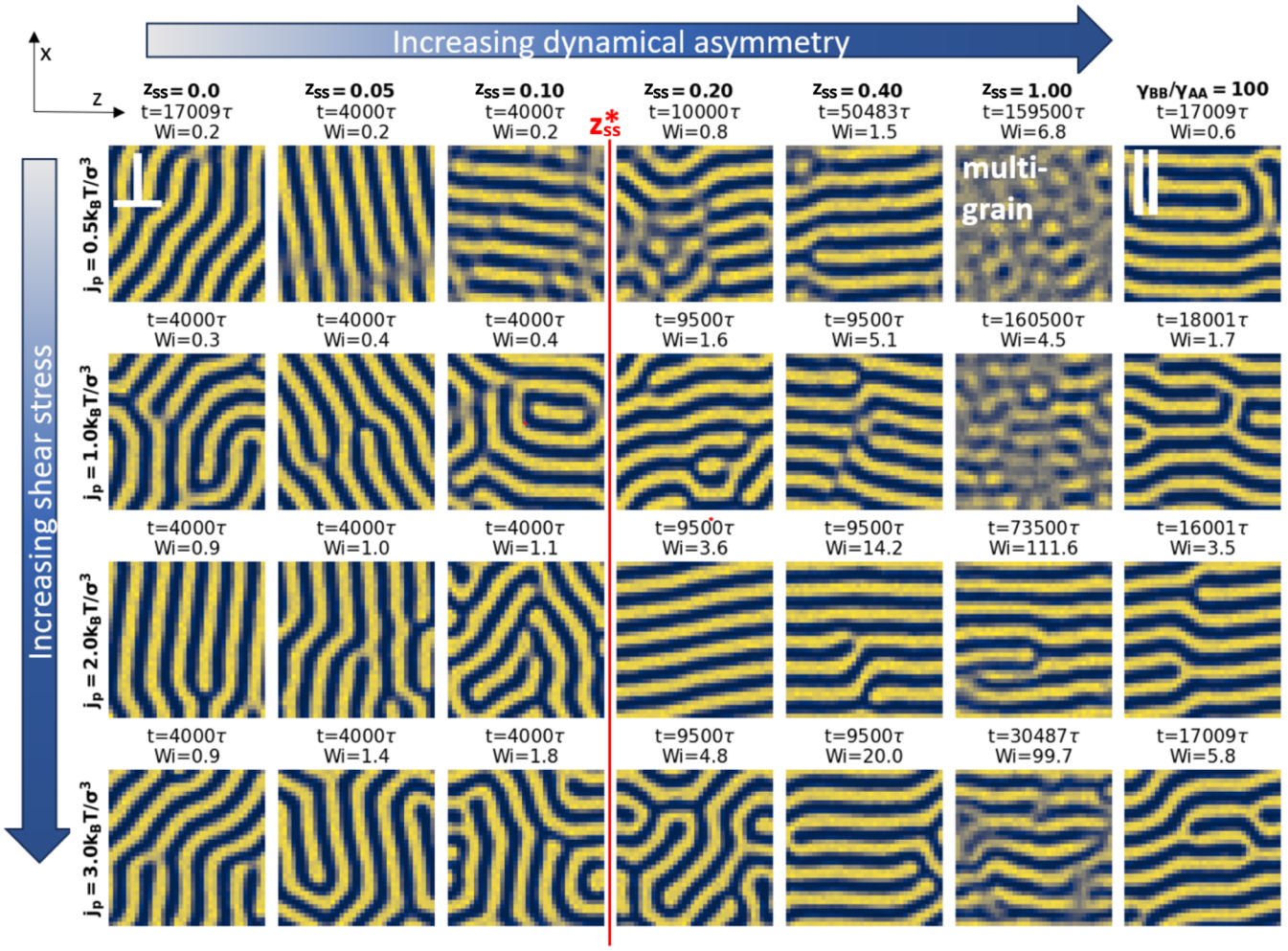

Figure 7. Snapshots illustrating the *A*-block density averaged along the shear-flow direction after quenching initially disordered systems to $\chi N \approx 40$ in a steady shear flow. The shear gradient is pointing in the vertical direction and the flow into the image plane. The dynamical asymmetry increases with the slip-spring activity, z_{ss}, from left to right. The right-most column depicts the results for strongly asymmetric segmental frictions, γ_{BB}/γ_{AA} = 100 with z_{ss} = 0. The shear stress, j_p, increases from top to bottom.

data in Figure 4 indicate that the switch of orientation occurs at $z_{ss}^* \approx 0.15$.

For z_{ss} = 1 and small $j_p \leq 1\ k_BT/\sigma^3$, the shear flow was not sufficient to generate a single-grain structure within the time t = 159 500$\tau \approx 15\tau_R$. Thus, the density, averaged along the shear-flow direction, does not exhibit a well-defined structure.

Slightly below the threshold value, $z_{ss} = 0.1 < z_{ss}^*$, and large shear stress, j_p, the system adopts the expected perpendicular orientation. At small shear stresses, $j_p \leq 1\ k_BT/\sigma^3$, however, we occasionally observe the parallel orientation. Note that the structure formation is a stochastic process and different realizations with the same thermodynamic starting and ending conditions may give rise to different outcomes. For better statistical significance, we repeated the simulations of the quench for the system with $z_{ss} = 0.1 < z_{ss}^*$ for small shear stresses $j_p \leq 1\ k_BT/\sigma^3$ four times for each of the selected shear stress. For $j_p = 0.5\ k_BT/\sigma^3$, we observed formation of the parallel orientation three times and observed formation of the perpendicular orientation once. For $j_p = 1k_BT/\sigma^3$, we observed formation of the parallel orientation for all four stochastic realizations of the quench, which does not comply with the prediction of the Rayleighian.

We hypothesize that once the metastable, parallel orientation has initially formed in the course of structure formation, the difference between the Rayleighians at weak shear is insufficient to reorient the incipient structure in the time window of our simulation. In the disordered state subjected to shear flow, the chains are primarily stretched along the *y*-direction of the flow (see Figure 6). This chain alignment favors the initial formation of lamellae with normals along the chain-stretching/shear-flow direction, *y*, i.e., the transverse orientation of lamellae. In Figure 8 we plot the time evolution of the peak of the collective structure factor of composition fluctuations, $\int_{q^{\mathrm{LAM}}-\delta q_-}^{q^{\mathrm{LAM}}+\delta q_+} \mathrm{d}q\ S(q)$, around the wave vector of the microphase-separation, $q^{\mathrm{LAM}} = \frac{2\pi}{L_0}$, along each of the three Cartesian directions for the selected system with z_{ss} = 0.1 and $j_p = 0.5\ k_BT/\sigma^3$. Indeed, one can appreciate that the scattering in the *y* direction, corresponding to the transverse orientation, is larger than the scattering in the other directions at $t > 500\tau$, after the incompatibility has been increased to χN = 40. This transverse orientation of the lamellae, however, is unstable because the lamellar sheets are continuously extended while their spacing is continuously compressed. Therefore, the scattering along the *y* direction decreases at later times, $t > 1000\tau$. The tilting of the transverse lamellae in the shear flow into the direction of the shear gradient results in parallel

https://doi.org/10.1021/acs.macromol.4c00943
Macromolecules 2024, 57, 8470−8486

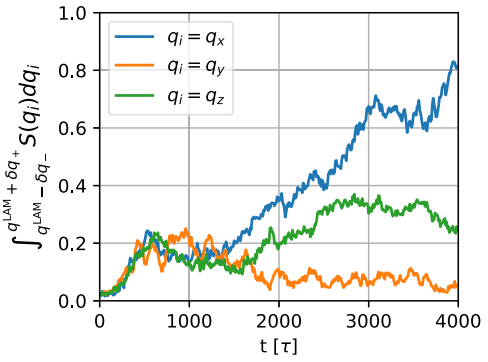

Figure 8. Average of the structure factor of composition fluctuations, $\int_{q_i^{LAM}-\delta q_-}^{q_i^{LAM}+\delta q_+} S(q_i)\mathrm{d}q_i$, for each dimension, $i \in [x, y, z]$, around the wave vector of lamellae, $\frac{2\pi}{12\sigma} = q_i^{LAM} - \delta q_- \le q_i \le q_i^{LAM} + \delta q_+ = \frac{2\pi}{5\sigma}$ as a function of time for the quenched system with $z_{ss} = 0.1$ and $j_p = 0.5\ k_BT/\sigma^3$. The initial, linear increase of the incompatibility occurs from $t = 0\tau$ until $t_Q = 500\tau$. The orientation of the wave vector corresponds to the lamellar normal, i.e., q_x, q_y, and q_z characterize the parallel, transverse, and perpendicular lamellar orientations, respectively. The transverse and the parallel orientation dominate at intermediate ($t \approx 1000\tau$) and late times, respectively.

oriented lamellae, i.e., the scattering along the x-direction increases. This geometric consideration suggests that the processing—initial shear in the disordered, homogeneous melt state, followed by a quench into the microphase-separated state—kinetically favors the formation of the metastable parallel orientation of lamellae although the Rayleighian predicts the perpendicular orientation to be stable.

Two Orthogonally Oriented Grains under Shear Flow. An alternative strategy to establish the stable orientation under steady shear consists in investigating a system that is comprised of two lamellar grains with different orientations. In the following, we study a large system that comprises two grains of 6 lamellae each. In the initial state, the lower grain is parallel oriented and the upper grain is perpendicularly aligned. We expect that the grain boundary moves, so as to expand the volume of the stable grain. The grain-boundary motion involves surmounting multiple free-energy barriers.[51] Thus, in the simulations of grain-boundary motion under shear, we have reduced the invariant degree of polymerization to $\sqrt{\bar{N}} = 19$ in order to reduce the free-energy scale of barriers, shifting the time scale of thermally activated changes of the domain morphology into the time window accessible to our simulations. Using the isotropy of the pressure, we have determined the equilibrium lamellar spacing to be, as expected, slightly smaller than in the previous section, $L_0 = (5.2 \pm 0.2)\sigma$, and we consider the system geometry $L_x \times L_y \times L_z = 64 \times 31 \times 31\sigma^3$. The smaller $\sqrt{\bar{N}}$ also results in a lower viscosity, $\eta \sim \sqrt{\bar{N}}$, and thereby leads to a higher shear rate or Weissenberg number at a given shear stress, j_p. Therefore, we consider only the interval $0.1 \le j_p\sigma^3/k_BT \le 1.0$.

In Figure 9 we present snapshots of the y-averaged A-block density after selected times. Again a prevalence for the perpendicular orientation can be found for small dynamical asymmetries, $z_{ss} \le 0.1$. For large asymmetries, $z_{ss} \ge 0.4$ or $\gamma_{BB}/\gamma_{AA} = 100$, in turn, the parallel orientation is mostly preferred. This behavior is in accord with the Rayleighian and the quench studies.

Only for the systems with $z_{ss} = 0.2$ or $\gamma_{BB}/\gamma_{AA} = 100$ and large shear stresses, we find the perpendicular orientation, not complying with the predictions of the Rayleighian. These exceptions can be rationalized as follows: First, the smaller invariant degree of polymerization $\sqrt{\bar{N}} = 19$ changes the ratio of the Rayleighians. For the system with $\gamma_{BB}/\gamma_{AA} = 100$, the ratio is decreased to $R_\parallel/R_\perp = 1.3 \pm 0.4$. For the systems with slip springs, the measured ratio of the Rayleighians is slightly higher at $\sqrt{\bar{N}} = 19$ than at $\sqrt{\bar{N}} = 32$, although the effective slip-spring density is smaller for the lower $\sqrt{\bar{N}} = 19$. We find $R_\parallel/R_\perp = 1.6 \pm 0.4$ for the system with $z_{ss} = 0.2$ and $\sqrt{\bar{N}} = 19$. Thus, the dynamical asymmetry of the two systems with $\gamma_{BB}/\gamma_{AA} = 100$ and $z_{ss} = 0.2$, is close to the switch of orientation predicted by the Rayleighian. In these cases, we observe that the orientation of the growing grain depends on the magnitude of the shear rate.

Second, at large shear rate, additional effects may come into play, promoting the perpendicular orientation, contrary to the prediction of the Rayleighian. In Table 3, we present the measured chains' mean-squared end-to-end distance projected onto the x- and z-directions for simulations of lamellar systems with lamellar normals oriented either parallel, i.e., along the x-axis, or perpendicular, i.e., along the z-axis, to the shear gradient. While the projected mean-squared chain extensions in the perpendicular lamellar orientation are rather unaffected by the shear, a small but statistically significant decrease of the chain extension in direction, x, of the shear gradient is observable for the parallel lamellar orientation.

Due to the fixed geometry of the simulation box, the lamellar spacing does not change, i.e., the all systems are comprised of 6 lamellae of thickness $L_0 = 5.16\sigma$, with or without shear flow. Nevertheless, the variation of chain extension, $R^2_{e,x}$, along the lamellar normal of the parallely oriented lamellae with shear rate indicates that the preferred lamellar spacing of the parallel oriented lamellae is shear-rate dependent, whereas the effect of shear on the preferred lamellar spacing in the perpendicular orientation is much weaker.

In the simulation of the grain-boundary motion, this effect tends to additionally destabilize the parallel lamellar orientation because its preferred lamellar spacing deviates from that imposed by the fixed simulation-box geometry at high shear stress, i.e., the perpendicular orientation is additionally stabilized at high shear by the fixed simulation-box geometry. Consequently, the transition from the perpendicular to the parallel orientation at high shear stress occurs at larger dynamical asymmetry. This rationale is supported by the observation of buckled parallel lamellae for $z_{ss} = 0.2$ and $j_P = 1k_BT/\sigma^3$, indicating that the preferred lamellar spacing is smaller that that imposed by the fixed simulation-box geometry.[68]

Finally, we investigate the mechanism, by which the stable lamellar orientation is established. Depending on the dynamical asymmetry and the magnitude of shear stress, we find different orientation mechanisms: (i) The stable grain grows via grain-boundary motion, (ii) the grain grows by a microemulsion-like pathway,[33] where the unstable grain becomes globally distorted and reintegrates into lamellae of stable orientation, or (iii) the grain grows by a combination of both mechanisms, when the time scales of both mechanisms are comparable. In the keys of Figure 9 we have indicated the observed transition pathway for each simulation. For small

https://doi.org/10.1021/acs.macromol.4c00943
Macromolecules 2024, 57, 8470−8486

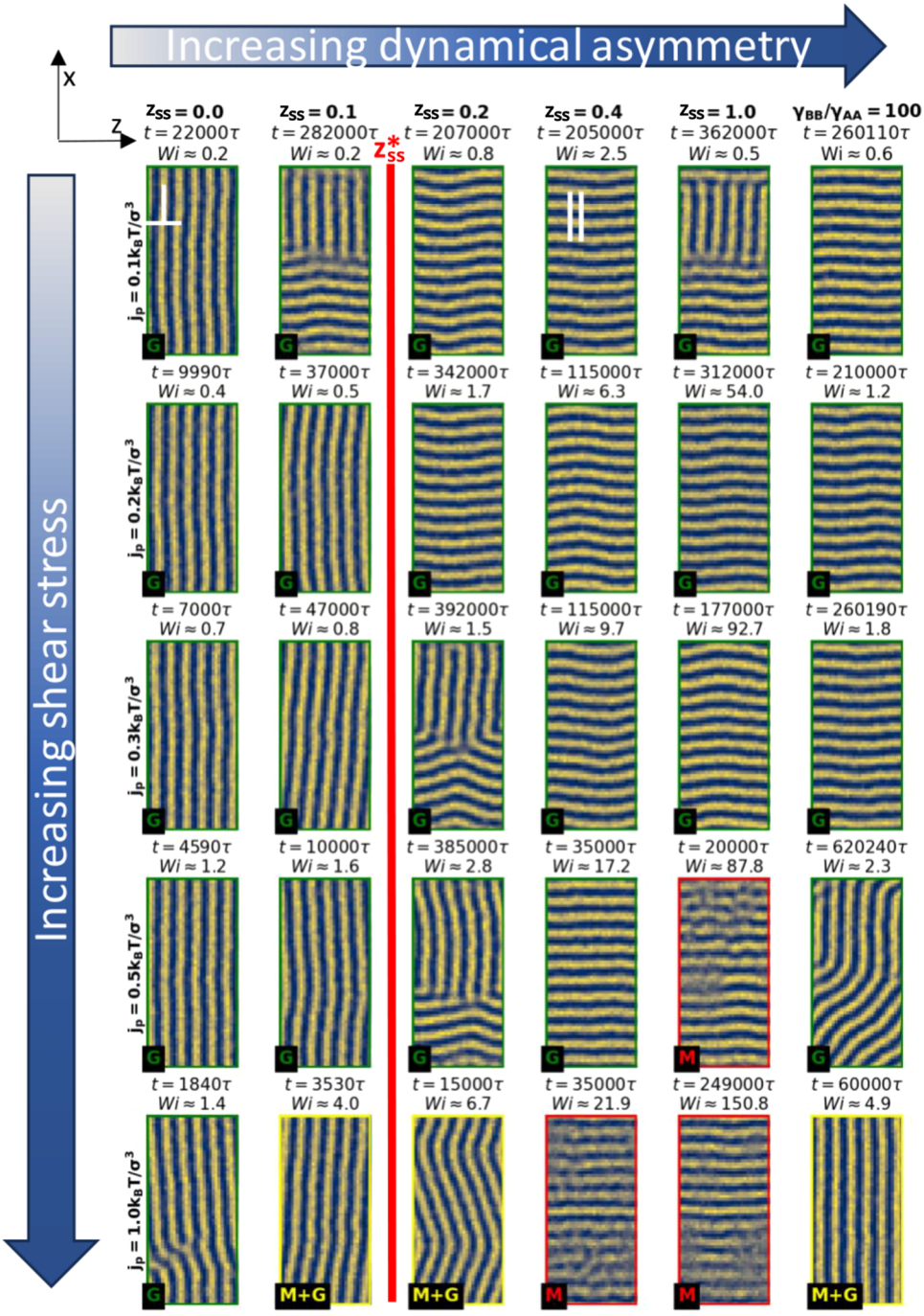

Figure 9. Density of *A*-blocks, averaged along the shear-flow direction with the shear gradient pointing in the vertical direction and the shear flow pointing into the image plane. Initially, the upper lamellar grain was perpendicularly oriented, whereas the lower grain adopted a parallel orientation. The snapshots depict the morphology at times indicated in the key for increasing shear stresses, j_p, from top to bottom and increasing slip-spring activities, z_{ss}, from left to right. The right-most column shows the results for γ_{BB}/γ_{AA} = 100 and z_{ss} = 0. The key marks the transition mechanism, where "**G**" corresponds to grain growth, "**M**" indicates a microemulsion-like pathway, and "**M** + **G**" denotes a combination of both mechanisms.

Weissenberg numbers, Wi ≪ 5, we mainly observe the grain-growth pathway. Exceptions are the systems with z_{ss} = 0.4 and z_{ss} = 1 where we observe the grain-growth pathway even at larger shear rate, Wi > 5. However, this Weissenberg number is measured at the shown time step. At earlier times, however, when the perpendicular grain is still intact, we find Wi < 5 for these systems (cf. Figure 10). Around Wi ≈ 5 we find a crossover between the grain-growth pathway and the micro-emulsion pathway, whereas for Wi ≫5 the microemulsion pathway becomes dominate.

In Figure 10 we present time series of the density for selected systems to illustrate the different transition mechanisms. Here, one can appreciate the increase of the Weissenberg number as the system transitions into the stable orientation at a fixed shear stress, maximizing the hydrodynamic energy dissipation and thereby supporting our

https://doi.org/10.1021/acs.macromol.4c00943
Macromolecules 2024, 57, 8470−8486

Table 3. Chains' Mean-Squared End-to-End Distance Projected onto the Shear-Gradient Axis, $R^2_{e,x}$, and the Axis Perpendicular to the Shear Flow and Shear Gradient, $R^2_{e,z}$, Measured for Systems with 6 Lamellae in a Volume of $(32\sigma)^3$ with $\sqrt{\bar{N}} = 19$ and $z_{ss} = 0.2$[a]

	parallel $j_p = 0\ k_BT/\sigma^3$	parallel $j_p = 1\ k_BT/\sigma^3$	perpendicular $j_p = 0\ k_BT/\sigma^3$	perpendicular $j_p = 1\ k_BT/\sigma^3$
$R^2_{e,x}$	4.96 ± 0.04	4.85 ± 0.05	2.99 ± 0.03	2.98 ± 0.03
$R^2_{e,z}$	2.99 ± 0.03	3.03 ± 0.03	4.96 ± 0.04	4.94 ± 0.04

[a]The lamellae are either oriented parallel to the shear gradient (normal vector parallel to x-direction), or perpendicular to it (normal vector parallel to z-direction) and the data is measured for simulations without shear and for systems subject to a constant shear stress with $j_p = 1k_BT/\sigma^3$, which results in Wi ≈ 3 for the parallel configuration and Wi ≈ 2 for the perpendicular orientation.

hypothesis that the minimization of the Rayleighian identifies the stable morphology of the nonequilibrium steady state.

EXPERIMENTAL RESULTS

Alignment Experiments for PS-*b*-P2VP. We align the lamellae of the PS-*b*-P2VP samples by applying steady or oscillatory shear with parallel plates. The temperature window for these experiments, displayed in Figure 11, is dictated by the requirement that the sample is liquid, $T > \max(T_{g,PS}, T_{g,PMMA}) = T_{g,PS}$ and forms lamellae, $T < T_{ODT}$. Close to the T_g of the polystyrene block—the component with the higher T_g—the polymer melt does not behave fluid-like, which limits the temperature range for rheological experiments and the choice of rheological parameters for the alignment experiments when approaching the upper T_g. The probability of sample failure, such as edge fracture, additionally increases when approaching the upper T_g, which is a reason why alignment experiments were limited to a short time frame.

Quenching from the Homogeneous Melt. To evaluate the stability of an orientation experimentally, the sample can be quenched from the homogeneous melt above the T_{ODT} under shear. By this procedure a prealignment i.e., resulting from sample handling when cooling from $T > T_{ODT}$ or flow caused by thermal contraction of the polymer melt, is completely absent. However, BCP melts display surface instabilities at the geometry edge when exposed to steady shear. Thus, alignment experiments could be conducted only for a limited time frame and shear rates $\dot{\gamma}$. The limiting temperatures, the

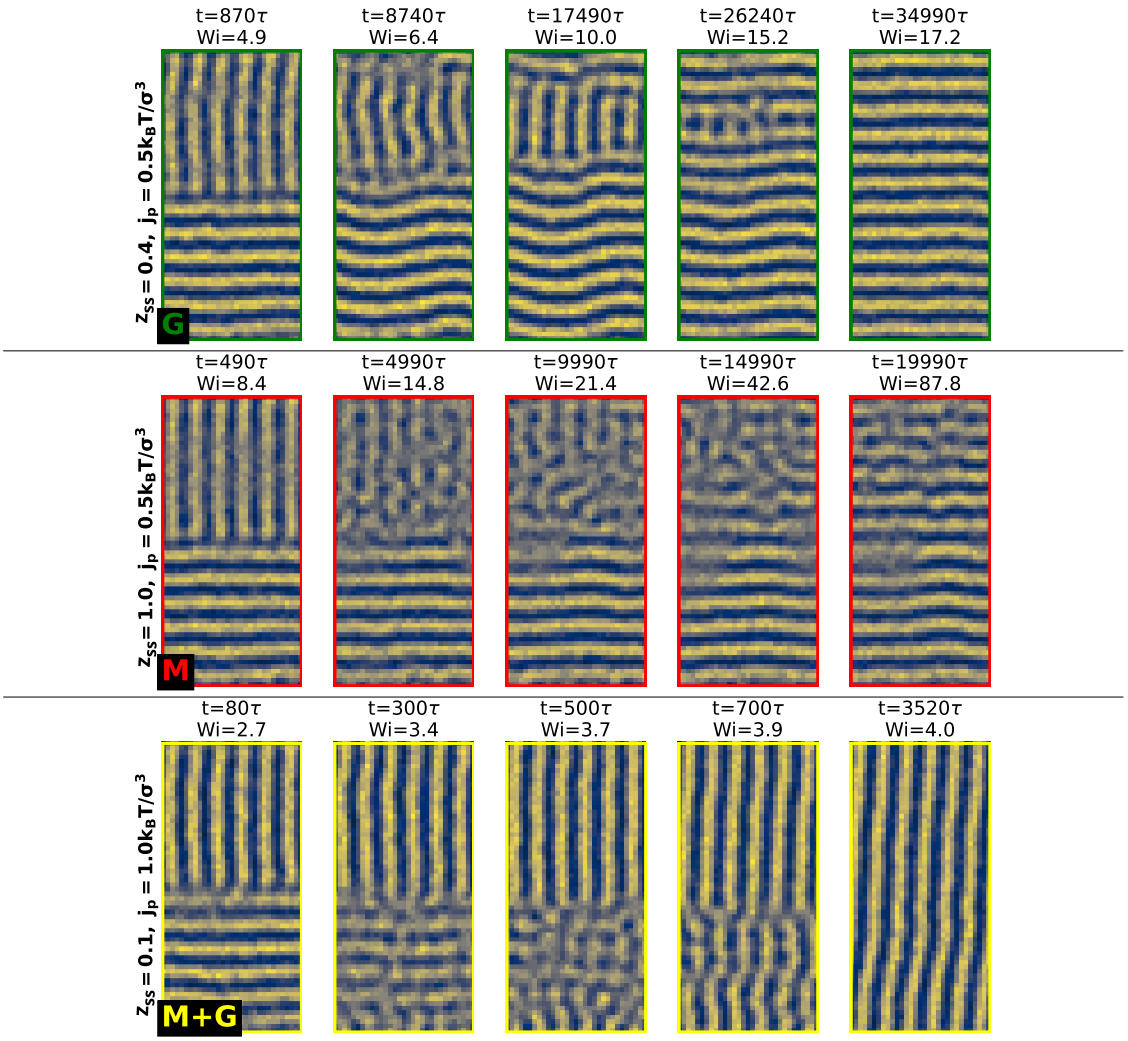

Figure 10. Time series of the *A*-block density, averaged along the shear-flow direction, for selected systems with two, orthogonally oriented grains in the initial state. The shear gradient points along the vertical axis and the shear flow into the image plane. The top row is an example of the grain-growth mechanism, **G**, the middle row shows a microemulsion-like pathway, **M**, and the bottom row displays a combination of both mechanisms, **M + G**.

https://doi.org/10.1021/acs.macromol.4c00943
Macromolecules 2024, 57, 8470−8486

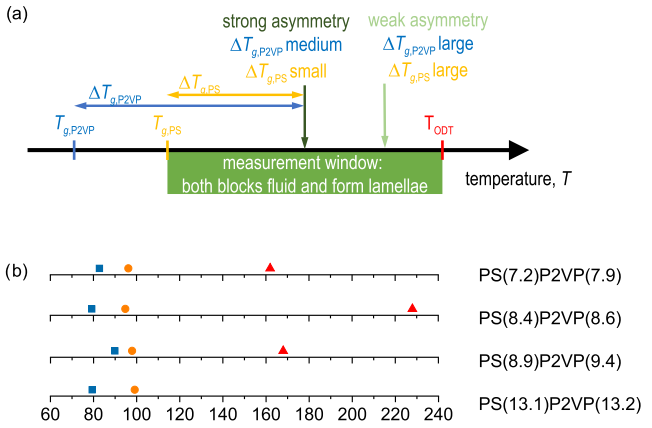

Figure 11. (a) Temperature window for domain-alignment experiments. We varied the mobility in the individual polymer blocks by experiments at different temperatures and thus unequal differences to the glass transition temperature T_g of the individual polymer blocks. (b) Temperature window for the individual polymer samples, which are listed in Table 2. The square, circle, and triangle symbols mark the T_g of the P2VP block, the T_g of the PS block, and the T_{ODT} of the sample, respectively.

T_g of the PS block and T_{ODT}, are mentioned at the respective sample in the following.

The sample PS(7.2)P2VP(7.9) ($T_{g,PS}$ = 96.2 °C, T_{ODT} = 162 °C) was quenched, applying steady shear of $\dot{\gamma}$ = 1 and 5 s^{-1} from T_{ODT} + 5 K to T_{ODT} − 5 K over 10 min and the parallel orientation was found for the higher shear rate, whereas the sample was nearly nonoriented for the lower $\dot{\gamma}$. The temperature range was limited to 10 K in order to reduce the probability of experimental problems, which increases drastically when cooling closer to the upper T_g of the polymer blocks. The observation of the parallel orientation for this dynamically asymmetric sample is in accord with our simulation result that the parallel orientation is favored for dynamically asymmetric polymers. For the discussion about polymer block mobility in the experimental systems, please refer to the subsequent section Sample Comparison.

The sample PS(8.9)P2VP(9.4) ($T_{g,PS}$ = 97.9 °C, T_{ODT} = 168 °C) can be considered dynamically asymmetric, but slightly more symmetric at T_{ODT} than the previous sample (PS(7.2)P2VP(7.9)), as both T_gs are close together and the T_{ODT} − 5 K is about 65 K above the T_g of PS. When quenched under steady shear with a shear rate of $\dot{\gamma}$ = 1 s^{-1} from T_{ODT} + 5 K to T_{ODT} − 5 K over 10 min the parallel orientation was observed. The formation of the parallel lamellar orientation after a quench from T_{ODT} in this sample confirms the stability of the parallel orientation for sufficient dynamical asymmetry and is in agreement with our simulations.

The sample PS(8.4)P2VP(8.6) ($T_{g,PS}$ = 96.2 °C, T_{ODT} = 226 °C) was quenched under steady shear with $\dot{\gamma}$ = 1, 3, and 5 s^{-1} from T_{ODT} + 5 K to T_{ODT} − 5 K over 10 min and an increasingly strong X-ray scattering signals relating to the perpendicular orientation was observed with increasing $\dot{\gamma}$. The sample PS(8.4)P2VP(8.6) has the largest difference between T_g and T_{ODT} due to a different synthetic procedure, see Synthesis, and thus the smallest dynamical asymmetry at T_{ODT} of the samples in this study. The formation of the perpendicular orientation for this rather dynamically symmetric BCP is in accord with the Rayleighian minimization and the simulations.

In summary the PS-*b*-P2VP samples exhibit a trend toward the parallel orientation for lower temperatures or higher dynamical asymmetry. This finding for a quench from the disordered state in the presence of shear is in accord with the stability prediction of the simulation via the Rayleighian, which predicts the parallel orientation for dynamically symmetric BCPs ($R_\parallel/R_\perp \approx 0.4$) and the perpendicular orientation for an increased dynamical asymmetry ($R_\parallel/R_\perp \approx 2.5$; see Shear Flow in Lamellar Configurations). The same trend toward the formation of the parallel orientation for increasing dynamical asymmetry was found for BCP melts with entanglements in their polymer blocks or in one of the polymer blocks in other studies.[24,69] Thus, the dynamical asymmetry as a guide toward the obtained domain orientation can be considered general, independent of the origin of the mobility difference in the polymer blocks.

Additionally, the orientation may be directed toward the perpendicular orientation by an increase of the steady shear rate, $\dot{\gamma}$. This situation resembles the structural formation after a quench in the simulation, in which we observed the formation of the expected perpendicular orientation in dynamically symmetric systems (refer to Quench from the Disordered State in the Presence of Shear Flow) for high shear stresses and the parallel orientation for low shear stresses.

A possible additional reason, which contributes to the formation of the parallel orientation at low shear rates in experiments, is the preferential adsorption of one polymer block to the metal surfaces of the measurement tools and formation of oriented grains parallel to this surface.[70] The surface-induced domain alignment is covered in the Supporting Information (SI) as it does not refer to the dynamical asymmetry as a cause of different lamellar orientations, but represents another guiding parameter toward the parallel orientation.

Realignment Experiments. The stability of the different orientations was examined by reorientation experiments. This corresponds to the order−order transition with two polymer grains in different orientations in the simulation, see section Two Orthogonally Oriented Grains under Shear Flow. In the realignment experiments, the lamellae were first aligned in one orientation at one temperature and then realigned at another temperature using the same strain amplitude and excitation frequency.

Probing experiments were conducted (see Figure SI7 in the SI) to find for the samples the experimental parameters for aligning the lamellae in two different orientations by only changing the temperature, and thus, change the mobility in the polymer blocks and the mobility difference between the polymer blocks. The lamellar orientation was determined by ex-situ SAXS experiments. The domain alignment was monitored in situ by broadband dielectric spectroscopy. For a detailed description of the used experimental setup, please refer to the literature.[71] For experimental details, please refer to the Supporting Information.

For the samples PS(8.4)P2VP(8.6) and PS(13.1)P2VP(13.2), the parallel orientation was found at comparable low temperatures (e.g., temperatures of 160 °C for PS(8.4)P2VP(8.6) and 190 °C for PS(13.1)P2VP(13.2)) and the perpendicular orientation at higher temperatures (e.g., temperatures above 180 °C for PS(8.4)P2VP(8.6) and 200 °C for PS(13.1)P2VP(13.2)), which translates to the finding of the parallel orientation for a high dynamical asymmetry and the perpendicular orientation for a lower dynamical asymmetry. This finding for the domain reorientation from an already oriented system is in accord with the stability prediction of the simulation via the Rayleighian, which predicts the parallel orientation for dynamically symmetric BCPs and the perpendicular orientation for an increased dynamical asymmetry, see Shear Flow in Lamellar Configurations. The experiments with the nonentangled polymer chains in the PS-*b*-P2VP melt is additionally in accord with studies on BCP melts with entanglements in both polymer blocks.[24] The temperature for the domain alignment and realignment experiments was chosen to be T = 160 and 180 °C respectively, so that the experiments would not be conducted too close to a critical temperature, which separates the two orientations as the most stable one. Conducting experiments close to a critical temperature may additionally increase the probability to align the lamellae to a metastable orientation.

In summary, the lamellae could be aligned in the different orientations depending on the temperature or the mobility difference in the polymer blocks, as is the case for the two orthogonally oriented polymer grains in Two Orthogonally Oriented Grains under Shear Flow.

Unlike in the simulation, no information on the orientation mechanism could be obtained using the experimental techniques available, but only a slower reorientation could be observed. This slower kinetic may be explained by the necessity to generate new defects in an already ordered system to achieve another orientation.

https://doi.org/10.1021/acs.macromol.4c00943
Macromolecules 2024, 57, 8470−8486

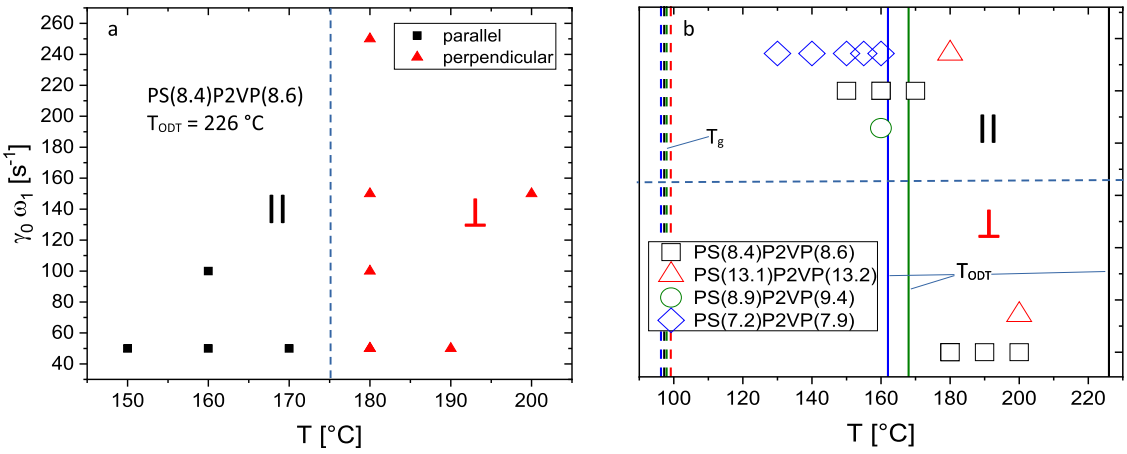

Figure 12. (a) Observed orientations for PS(8.4)P2VP(8.6) in alignment experiments with $\omega_1/2\pi$ = 1−10 Hz and γ_0 = 25−150% (b) Comparison of the orientation in multiple PS-*b*-P2VP samples with no entanglements in the polymer blocks. The values of T_g and T_{ODT} for the individual samples are indicated as dashed and solid vertical lines, respectively. A general trend toward the parallel orientation for low temperatures is evident.

As an example, in the displayed alignment experiments the absolute value of the complex viscosity $|\eta^*|$ changes by a factor of $f \approx 2$ in the initial alignment experiment at T = 180 °C, whereas $f \approx 1.3$ in the realignment experiment from the parallel orientation at the same temperature. The complex viscosity is a measure of the total resistance to flow as a function of angular frequency and is given by the quotient of the maximum stress amplitude and maximum strain rate amplitude and is defined as $|\eta^*| = |G^*|/\omega_1$. The complex modulus G^* is a quantitative measure of material stiffness or resistance to deformation and can be defined as the sum of the real part of the storage modulus G' and the imaginary part of the loss modulus G''as follows $G^* = G' + iG''$.

Sample Comparison. Although there are regions of differently aligned lamellae within one sample, a critical temperature, T^*, at which a transition from the parallel to the perpendicular orientation as the most stable one can be determined for some samples. For other samples, only the parallel orientation was found due to a limited temperature range for the alignment experiments, and thus similar mobility of the polymer blocks in these experiments, see Figure 11. The determined orientations of PS(8.4)P2VP(8.6) are displayed in Figure 12a.

The stress in the system, which results from γ_0 and ω_1, did not result in different orientations if $\gamma_0 \cdot \omega_1$ increased from 40 to 250 s^{-1} close to T^* at T = 180 °C in our study. An increase of γ_0 and ω_1 appear to exhibit only a subordinate role close to T^* for the domain alignment of the nonentangled PS-*b*-P2VP in this study. If compared to other nonentangled PS-*b*-P2VP samples, like displayed in Figure 12b, only an increase of T^* with molecular weight can be noticed.

In order to generalize the critical temperatures T^* in Figure 12 and to obtain an universal abscissa similar to Figure 5, we calculated the viscosity η of the PS and P2VP blocks and used the ratio η_{P2VP}/η_{PS}. We omitted the use of τ to calculate the mobility ratio due to large errors resulting from extrapolation of relaxation times determined from entangled homopolymers to the relaxation time of nonentangled polymer blocks. We used the viscosity of nonentangled homopolymers with molecular weights of 9000 g/mol (PS) and 9500 g/mol(P2VP) for T = 140 °C, which is close to our experimental situation and used as a reference temperature T_{ref}.[59] The viscosity was shifted to the temperature of the alignment experiments using time−temperature superposition and the William-Landell Ferry equation $\log a_T = (-C_1(T - T_{ref}))/(C_2 + (T - T_{ref}))$ with C_1 = 7.455 and C_2 = 131.4 K for PS and C_1 = 6.828 and C_2 = 121.4 K for P2VP and T_{ref} = 160 °C.[72] We further adapted the temperature of the alignment experiment T_{exp} using the T_g of the individual polymer block $T_{g,block}$, see Table 2, and T_g = 100.8 °C as the T_g for high molecular weight P2VP. The heat flow curve of P2VP can be found in the Supporting Information (see Figure SI5). We did not observe an universal critical viscosity ratio $(\eta_{P2VP}/\eta_{PS})^*$, below which the perpendicular orientation and above which the parallel orientation is obtained, but $(\eta_{P2VP}/\eta_{PS})^*$ for PS(8.4)P2VP(8.6) ($(\eta_{P2VP}/\eta_{PS})^*$ = 1.20) and for PS(13.1)P2VP(13.2) ($(\eta_{P2VP}/\eta_{PS})^*$ = 1.17) is in the same range and also in a similar range as in the simulations (25), please compare to section Shear Flow in Lamellar Configurations. Experimentally a critical viscosity ratio $(\eta_{P2VP}/\eta_{PS})^*$, can be approximated. The lamellar orientation changes from a perpendicular orientation toward a parallel orientation around a value of $(\eta_{P2VP}/\eta_{PS})^*$ = 1.04−1.3.

Please note that the absolute value of $(\eta_{P2VP}/\eta_{PS})^*$ has to be considered with caution as it is highly dependent on the T_g of the PS and P2VP homopolymer and the T_g of the individual polymer blocks. A similar T_g of PS and P2VP and the dependence of T_g on the degree of separation, see Figure SI18 in the SI, complicates their exact determination and thus the difference to T_{exp} for individual samples. Uncertainties in the T_g of individual polymer blocks and samples results in different values of $(\eta_{P2VP}/\eta_{PS})^*$ for different samples. For a description of their calculation, please refer to Calculation of the viscosity ratio in the SI. Critical values between the parallel and perpendicular orientation were not determined for the other two samples in this study. Due to their comparable low T_{ODT}, alignment experiments were limited to low temperatures, see Figure 11, at which the parallel orientation was found, see Quenching from the Homogeneous Melt. This result confirms the trend toward the parallel orientation for a high dynamical asymmetry, as predicted by the simulation. However, a determination of T^* or $(\eta_{P2VP}/\eta_{PS})^*$, respectively, is obviously not possible for these samples.

The formation of the different orientations, being a function of temperature and also the viscosity ratio η_{P2VP}/η_{PS} can be explained by different mechanisms, such as a layer-sliding mechanism for large η_{P2VP}/η_{PS}, as can be seen in the velocity profile of the parallel orientation in Figure 4. For the same rheological parameters (γ_0, ω_1) but a higher temperature or lower η_{P2VP}/η_{PS}, respectively, the formation of the perpendicular orientation is favored. This can be explained by the energy dissipation via both polymer blocks, when the junction point between the polymer blocks can move along the phase boundary in the direction of the shear flow and the velocity gradient equally.

SUMMARY AND CONCLUSIONS

We have performed MD simulations of lamellae-forming diblock copolymers under shear, using a highly coarse-grained model. Whereas the structure and thermodynamics of the two blocks are symmetric, we have controlled the dynamical asymmetry of the two blocks either by (i) increasing the segmental friction, γ_{BB}/γ_{AA} of the slower *B*-block, or by (ii) adding slip springs with activity z_{ss} to the *B*-block that mimic entanglements inside the domain of the slow block. System-

https://doi.org/10.1021/acs.macromol.4c00943
Macromolecules 2024, 57, 8470−8486

atically varying the dynamical asymmetry, we investigated the stability of different lamellar orientations with respect to the shear flow by (i) minimizing the Rayleighian, (ii) observing the structure formation after a quench from the disordered state, and (iii) studying the grain growth in a system initially comprised of a parallel and a perpendicular lamellar grain. We observed that for dynamically symmetric diblock copolymers the perpendicular orientation is stable in steady shear, in accord with previous simulation studies.[28,33] For large dynamical asymmetry, however, the parallel orientation becomes the stable, nonequilibrium steady state. These findings are independent from the mechanism by which the dynamical asymmetry is created, and our simulations suggest that the switch from perpendicular to parallel orientation occurs when the ratio of the relaxation times of the blocks exceeds an order of magnitude. In the ultimate vicinity of the switch from perpendicular to parallel orientation, we have identified additional effects: (i) The chain stretching along the shear-flow direction in the sheared, disordered state before a quench below the ODT favors the parallel orientation and (ii) the shear-stress dependence of the lamellar spacing (in a multigrain system of fixed geometry) favors the perpendicular state at large shear rates.

In the experiment, we used the block copolymer (BCP) system polystyrene-*b*-poly-2-vinylpyridine (PS-*b*-P2VP), where the difference in the glass transition temperature is $\Delta T_g \approx 15$ °C to correlate the computer simulation with experimental polymer systems in alignment experiments. Varying the temperatures to generate different distances to both T_gs, consequently allows to influence the mobility in the polymer blocks unequally and thus tune the dynamical asymmetry from a symmetric system at high temperatures toward an asymmetric system at lower temperatures, closer to both T_gs. We designed the polymer alignment experiments to be similar to the computer-simulated ones, i.e., quenching from the homogeneous melt. We could confirm the formation of the perpendicular orientation for high dynamical asymmetries and the perpendicular orientation for dynamically more symmetric BCP melts.

■ ASSOCIATED CONTENT

Supporting Information

The Supporting Information is available free of charge at https://pubs.acs.org/doi/10.1021/acs.macromol.4c00943.

Additional information on parameter choice, synthesis, sample information, and realignment experiments (PDF)

■ AUTHOR INFORMATION

Corresponding Authors

Manfred Wilhelm − *Institute for Chemical Technology and Polymer Chemistry, Karlsruhe Institute for Technology, 76131 Karlsruhe, Germany;* orcid.org/0000-0003-2105-6946; Email: Manfred.wilhelm@kit.edu

Marcus Müller − *Institute for Theoretical Physics, Georg-August University, 37077 Göttingen, Germany;* orcid.org/0000-0002-7472-973X; Email: mmueller@theorie.physik.uni-goettingen.de

Authors

Niklas Blagojevic − *Institute for Theoretical Physics, Georg-August University, 37077 Göttingen, Germany;* orcid.org/0000-0002-7399-8671

Matthias Heck − *Institute for Chemical Technology and Polymer Chemistry, Karlsruhe Institute for Technology, 76131 Karlsruhe, Germany;* orcid.org/0000-0002-7752-1838

Complete contact information is available at: https://pubs.acs.org/10.1021/acs.macromol.4c00943

Notes

The authors declare no competing financial interest.

■ ACKNOWLEDGMENTS

This work was supported by the German Science Foundation (DFG) under grants Mu 1674/17-2 and Wi 1911/22-2. The authors gratefully acknowledge the Gauss Centre for Supercomputing e.V. (www.gauss-centre.eu) for funding this research project by providing computing time through the John von Neumann Institute for Computing (NIC) on the GCS Supercomputer JUWELS/JUWELS BOOSTER at Jülich Supercomputing Centre (JSC) as well as the HLRN Berlin/Göttingen and the GoeGrid cluster at the University of Göttingen, which is supported by the Deutsche Forschungsgemeinschaft (project ID 436382789).

■ REFERENCES

(1) Matsen, M. W. The standard Gaussian model for block copolymer melts. *J. Phys.: Condens. Matter* **2002**, *14*, R21−R47.

(2) Müller, M.; de Pablo, J. J. Computational Approaches for the Dynamics of Structure Formation in Self-Assembling Polymeric Materials. *Annu. Rev. Mater. Res.* **2013**, *43*, 1−34.

(3) Li, W.; Müller, M. Defects in the Self-Assembly of Block Copolymers and Their Relevance for Directed Self-Assembly. *Annu. Rev. Chem. Biomol. Eng.* **2015**, *6*, 187−216.

(4) Amundson, K.; Helfand, E.; Davis, D. D.; Quan, X.; Patel, S. S.; Smith, S. D. Effect of an Electric Field on Block Copolymer Microstructure. *Macromolecules* **1991**, *24*, 6546−6548.

(5) Amundson, K.; Helfand, E.; Quan, X.; Smith, S. D. Alignment of lamellar block copolymer microstructure in an electric field. 1. Alignment kinetics. *Macromolecules* **1993**, *26*, 2698−2703.

(6) Amundson, K.; Helfand, E.; Quan, X.; Hudson, S. D.; Smith, S. D. Alignment of Lamellar Block Copolymer Microstructure in an Electric Field. 2. Mechanisms of Alignment. *Macromolecules* **1994**, *27*, 6559−6570.

(7) Thurn-Albrecht, T.; DeRouchey, J.; Russel, T. P.; Jaeger, H. M. Overcoming Interfacial Interactions with Electric Fields. *Macromolecules* **2000**, *33*, 3250−3253.

(8) Böker, A.; Knoll, A.; Elbs, H.; Abetz, V.; Müller, A. H. E.; Krausch, G. Large Scale Domain Alignment of a Block Copolymer from Solution Using Electric Fields. *Macromolecules* **2002**, *35*, 1319−1325.

(9) Kyrylyuk, A. V.; Zvelindovsky, A. V.; Sevink, G. J. A.; Fraaije, J. G. E. M. Lamellar Alignment of Diblock Copolymers in an Electric Field. *Macromolecules* **2002**, *35*, 1473−1476.

(10) Tsori, Y.; Andelman, D. Thin Film Diblock Copolymers in Electric Field: Transition from Perpendicular to Parallel Lamellae. *Macromolecules* **2002**, *35*, 5161−5170.

(11) Xu, T.; Hawker, C. J.; Russell, T. P. Interfacial Energy Effects on the Electric Field Alignment of Symmetric Diblock Copolymers. *Macromolecules* **2003**, *36*, 6178−6182.

(12) Xu, T.; Zvelindovsky, A. V.; Sevink, G. J. A.; Lyakhova, K. S.; Jinnai, H.; Russell, T. P. Electric Field Alignment of Asymmetric Diblock Copolymer Thin Films. *Macromolecules* **2005**, *38*, 10788−10798.

(13) Matsen, M. W. Converting the nanodomains of a diblock-copolymer thin film from spheres to cylinders with an external electric field. *J. Chem. Phys.* **2006**, *124*, No. 074906.
(14) Matsen, M. W. Electric Field Alignment in Thin Films of Cylinder-Forming Diblock Copolymer. *Macromolecules* **2006**, *39*, 5512−5520.
(15) Ly, D. Q.; Honda, T.; Kawakatsu, T.; Zvelindovsky, A. V. Hexagonally Perforated Lamella-to-Cylinder Transition in a Diblock Copolymer Thin Film under an Electric Field. *Macromolecules* **2008**, *41*, 4501−4505.
(16) Tsori, Y. Colloquium: Phase transitions in polymers and liquids in electric fields. *Rev. Mod. Phys.* **2009**, *81*, 1471−1494.
(17) Sevink, G. J. A.; Pinna, M.; Langner, K. M.; Zvelindovsky, A. V. Selective disordering of lamella-forming diblock copolymers under an electric field. *Soft Matter* **2011**, *7*, 5161−5170.
(18) Welling, U.; Muller, M.; Shalev, H.; Tsori, Y. Block copolymer ordering in cylindrical capacitors. *Macromolecules* **2014**, *47*, 1850−1864.
(19) Welling, U.; Müller, M. Ordering block copolymers with structured electrodes. *Soft Matter* **2017**, *13*, 486−495.
(20) Pester, C. W.; Liedel, C.; Ruppel, M.; Böker, A. Block copolymers in electric fields. *Prog. Polym. Sci.* **2017**, *64*, 182−214.
(21) Dreyer, O.; Schneider, L.; Radjabian, M.; Abetz, V.; Müller, M. Evaporation-Induced Self-Assembly of Diblock Copolymer Films in an Electric Field: A Simulation Study. *Macromolecules* **2023**, *56*, 6880−6890.
(22) Grigorova, T.; Pispas, S.; Hadjichristidis, N.; Thurn-Albrecht, T. Magnetic Field Induced Orientation in Diblock Copolymers with One Crystallizable Block. *Macromolecules* **2005**, *38*, 7430−7433.
(23) Tao, Y.; Zohar, H.; Olsen, B. D.; Segalman, R. A. Hierarchical Nanostructure Control in Rod-Coil Block Copolymers with Magnetic Fields. *Nano Lett.* **2007**, *7*, 2742−2746.
(24) Koppi, K. A.; Tirrell, M.; Bates, F. S.; Almdal, K.; Colby, R. H. Lamellae orientation in dynamically sheared diblock copolymer melts. *J. Phys. II* **1992**, *2*, 1941−1959.
(25) Wiesner, U. Lamellar diblock copolymers under large amplitude oscillatory shear flow: Order and dynamics. *Macromol. Chem. Phys.* **1997**, *198*, 3319−3352.
(26) Pryamitsyn, V.; Ganesan, V. Correlations in Block Copolymers under Shear. *Macromolecules* **2002**, *35*, 9847−9850.
(27) Fraser, B.; Denniston, C.; Müser, M. H. Diffusion, elasticity, and shear flow in self-assembled block copolymers: A molecular dynamics study. *J. Polym. Sci., Polym. Phys.* **2005**, *43*, 970−982.
(28) Fraser, B.; Denniston, C.; Müser, M. H. On the orientation of lamellar block copolymer phases under shear. *J. Chem. Phys.* **2006**, *124*, 104902.
(29) Liu, W.; Qian, H.-J.; Lu, Z.-Y.; Li, Z.-S.; Sun, C.-C. Dissipative particle dynamics study on the morphology changes of diblock copolymer lamellar microdomains due to steady shear. *Phys. Rev. E* **2006**, *74*, 021802.
(30) Peters, B. L.; Ramírez-Hernández, A.; Pike, D. Q.; Müller, M.; de Pablo, J. J. Nonequilibrium Simulations of Lamellae Forming Block Copolymers under Steady Shear: A Comparison of Dissipative Particle Dynamics and Brownian Dynamics. *Macromolecules* **2012**, *45*, 8109−8116.
(31) Shagolsem, L. S.; Kreer, T.; Sommer, J.-U. Shear-Induced Ordering in Thin Films of Diblock Copolymer Melts. *ACS Macro Lett.* **2014**, *3*, 1201−1204.
(32) Shagolsem, L. S.; Kreer, T.; Galuschko, A.; Sommer, J.-U. Diblock-copolymer thin films under shear. *J. Chem. Phys.* **2016**, *145*, 164908.
(33) Schneider, L.; Heck, M.; Wilhelm, M.; Müller, M. Transitions between Lamellar Orientations in Shear Flow. *Macromolecules* **2018**, *51*, 4642−4659.
(34) Müller, M. Process-directed self-assembly of copolymers: Results of and challenges for simulation studies. *Prog. Polym. Sci.* **2020**, *101*, 101198.
(35) Zhang, Y.; Wiesner, U.; Spiess, H. W. Frequency Dependence of Orientation in Dynamically Sheared Diblock Copolymers. *Macromolecules* **1995**, *28*, 778−781.
(36) Zhang, Y.; Wiesner, U. Symmetric diblock copolymers under large amplitude oscillatory shear flow: Entanglement effect. *J. Chem. Phys.* **1995**, *103*, 4784−4793.
(37) Schneider, L.; Müller, M. Rheology of symmetric diblock copolymers. *Comput. Mater. Sci.* **2019**, *169*, 109107.
(38) Groot, R. D.; Warren, P. B. Dissipative Particle Dynamics: Bridging the Gap Between Atomistic and Mesoscopic Simulation. *J. Chem. Phys.* **1997**, *107*, 4423−4435.
(39) Ramírez-Hernández, A.; Detcheverry, F. A.; Peters, B. L.; Chappa, V. C.; Schweizer, K. S.; Müller, M.; de Pablo, J. J. Dynamical Simulations of Coarse Grain Polymeric Systems: Rouse and Entangled Dynamics. *Macromolecules* **2013**, *46*, 6287−6299.
(40) Español, P.; Warren, P. B. Perspective: Dissipative particle dynamics. *J. Chem. Phys.* **2017**, *146*, No. 150901.
(41) Behbahani, A. F.; Schneider, L.; Rissanou, A.; Chazirakis, A.; Bačová, P.; Jana, P. K.; Li, W.; Doxastakis, M.; Polińska, P.; Burkhart, C.; Müller, M.; Harmandaris, V. A. Dynamics and Rheology of Polymer Melts via Hierarchical Atomistic, Coarse-Grained, and Slip-Spring Simulations. *Macromolecules* **2021**, *54*, 2740−2762.
(42) Li, W.; Jana, P. K.; Behbahani, A. F.; Kritikos, G.; Schneider, L.; Polińska, P.; Burkhart, C.; Harmandaris, V. A.; Müller, M.; Doxastakis, M. Dynamics of Long Entangled Polyisoprene Melts via Multiscale Modeling. *Macromolecules* **2021**, *54*, 8693−8713.
(43) Hollborn, K.-U.; Schneider, L.; Müller, M. Effect of Slip-Spring Parameters on the Dynamics and Rheology of Soft, Coarse-Grained Polymer Models. *J. Phys. Chem. B* **2022**, *126*, 6725−6739.
(44) Müller-Plathe, F. Reversing the perturbation in nonequilibrium molecular dynamics: An easy way to calculate the shear viscosity of fluids. *Phys. Rev. E* **1999**, *59*, 4894.
(45) Español, P.; Warren, P. Statistical Mechanics of Dissipative Particle Dynamics. *Europhys. Lett.* **1995**, *30*, 191.
(46) Chappa, V. C.; Morse, D. C.; Zippelius, A.; Müller, M. Translationally Invariant Slip-Spring Model for Entangled Polymer Dynamics. *Phys. Rev. Lett.* **2012**, *109*, 148302.
(47) Doi, M. Onsager's variational principle in soft matter. *J. Phys.: Condens. Matter* **2011**, *23*, 284118.
(48) Williams, M. L.; Landel, R. F.; Ferry, J. D. The Temperature Dependence of Relaxation Mechanisms in Amorphous Polymers and Other Glass-forming Liquids. *J. Am. Chem. Soc.* **1955**, *77*, 3701−3707.
(49) Ferry, J. D.; Landel, R. F. Molecular friction coefficients in polymers and their temperature dependence. *Kolloid Z.* **1956**, *148*, 1−6.
(50) Bueche, F. Derivation of the WLF Equation for the Mobility of Molecules in Molten Glasses. *J. Chem. Phys.* **1956**, *24*, 418−419.
(51) Blagojevic, N.; Müller, M. Multiscale Modeling of Grain-Boundary Motion in Cylinder-Forming Block Copolymers. *ACS Polym. Au* **2023**, *3*, 96−117.
(52) Swope, W. C.; Andersen, H. C.; Berens, P. H.; Wilson, K. R. A computer simulation method for the calculation of equilibrium constants for the formation of physical clusters of molecules: Application to small water clusters. *J. Chem. Phys.* **1982**, *76*, 637−649.
(53) Anderson, J. A.; Lorenz, C. D.; Travesset, A. General purpose molecular dynamics simulations fully implemented on graphics processing units. *J. Comput. Phys.* **2008**, *227*, 5342−5359.
(54) Phillips, C. L.; Anderson, J. A.; Glotzer, S. C. Pseudo-random number generation for Brownian Dynamics and Dissipative Particle Dynamics simulations on GPU devices. *J. Comput. Phys.* **2011**, *230*, 7191−7201.
(55) Ramírez-Hernández, A.; Peters, B. L.; Schneider, L.; Andreev, M.; Schieber, J. D.; Müller, M.; de Pablo, J. J. A multi-chain polymer slip-spring model with fluctuating number of entanglements: Density fluctuations, confinement, and phase separation. *J. Chem. Phys.* **2017**, *146*, No. 014903.
(56) Ramírez-Hernández, A.; Peters, B. L.; Schneider, L.; Andreev, M.; Schieber, J. D.; Muller, M.; Kroger, M.; de Pablo, J. J. A detailed

https://doi.org/10.1021/acs.macromol.4c00943
Macromolecules 2024, 57, 8470−8486

examination of the topological constraints of lamellae-forming block copolymers. *Macromolecules* **2018**, *51*, 2110−2124.
(57) Hadjichristidis, N.; Iatrou, H.; Pispas, S.; Pitsikalis, M. Anionic polymerization: high vacuum techniques. *J. Poly. Sci. Polym. Chem.* **2000**, *38*, 3211−3234.
(58) Hadjichristidis, N.; Pispas, S.; Floudas, G. *Block Copolymers: Synthetic Strategies, Physical Properties, and Applications*; John Wiley & Sons, 2003.
(59) Heck, M.; Schneider, L.; Müller, M.; Wilhelm, M. Diblock Copolymers with Similar Glass Transition Temperatures in Both Blocks for Comparing Shear Orientation Processes with DPD Computer Simulations. *Macromol. Chem. Phys.* **2018**, *219*, 1700559.
(60) Watanabe, H.; Amemiya, T.; Shimura, T.; Kotaka, T. Anionic Synthesis of Graft Block Copolymers with Poly(2-vinylpyridine) Trunks: Effects of Trunk and Branch Molecular Weights. *Macromolecules* **1994**, *27*, 2336−2338.
(61) Hadjichristidis, N.; Pitsikalis, M.; Pispas, S.; Iatrou, H. Polymers with Complex Architecture by Living Anionic Polymerization. *Chem. Rev.* **2001**, *101*, 3747−3792.
(62) Munam, A.; Gauthier, M. Large-scale synthesis of arborescent polystyrenes. *J. Polym. Sci., Part A: Polym. Chem.* **2008**, *46*, 5742−5751.
(63) Gausepohl, H.; Oepen, S.; Knoll, K.; Schneider, M.; McKee, G.; Loth, W. Super-polystyrene: a new class of engineering plastics with versatile properties. *Des. Monomers Polym.* **2000**, *3*, 299−315.
(64) Hyun, K.; Höfl, S.; Kahle, S.; Wilhelm, M. Polymer motion as detected via dielectric spectra of 1,4-cis-polyisoprene under large amplitude oscillatory shear (LAOS). *J. Non-Newtonian Fluid Mech.* **2009**, *160*, 93−103.
(65) Iacob, C.; Heck, M.; Wilhelm, M. Molecular Dynamics of Polymyrcene: Rheology and Broadband Dielectric Spectroscopy on a Stockmayer Type A Polymer. *Macromolecules* **2023**, *56*, 188−197.
(66) Meins, T.; Dingenouts, N.; Kübel, J.; Wilhelm, M. *In Situ* Rheodielectric, *ex Situ* 2D-SAXS, and Fourier Transform Rheology Investigations of the Shear-Induced Alignment of Poly(styrene- *b* −1,4-isoprene) Diblock Copolymer Melts. *Macromolecules* **2012**, *45*, 7206−7219.
(67) Bruns, W.; Carl, W. Chain extension in steady shear flow. *Macromolecules* **1993**, *26*, 557−558.
(68) Wang, Z.-G. Response and instabilities of the lamellar phase of diblock copolymers under uniaxial stress. *J. Chem. Phys.* **1994**, *100*, 2298−2309.
(69) Wang, H.; Kesani, P. K.; Balsara, N. P.; Hammouda, B. Undulations and Disorder in Block Copolymer Lamellae under Shear Flow. *Macromolecules* **1997**, *30*, 982−992.
(70) Balsara, N. P.; Hammouda, B.; Kesani, P. K.; Jonnalagadda, S. V.; Straty, G. C. In-Situ Small-Angle Neutron Scattering from a Block Copolymer Solution under Shear. *Macromolecules* **1994**, *27*, 2566−2573.
(71) Hyun, K.; Höfl, S.; Kahle, S.; Wilhelm, M. Polymer motion as detected via dielectric spectra of 1,4-cis-polyisoprene under large amplitude oscillatory shear (LAOS). *J. Non-Newtonian Fluid Mech.* **2009**, *160*, 93−103.
(72) Cziep, M. A.; Abbasi, M.; Heck, M.; Arens, L.; Wilhelm, M. Effect of Molecular Weight, Polydispersity, and Monomer of Linear Homopolymer Melts on the Intrinsic Mechanical Nonlinearity $^3Q_0(\omega)$ in MAOS. *Macromolecules* **2016**, *49*, 3566−3579.

https://doi.org/10.1021/acs.macromol.4c00943
Macromolecules 2024, 57, 8470−8486